Interfacial Interactions of Polymer Brushes in Restricted Geometries

By

WEI-PO LIAO
B.S. (National Chung-Hsing University) 2000
M.S. (National Cheng-Kung University) 2002

DISSERTATION

Submitted in partial satisfaction of the requirements for the degree of

DOCTOR OF PHILOSOPHY

in

Materials Science and Engineering

in the

OFFICE OF GRADUATE STUDIES

of the

UNIVERSITY OF CALIFORNIA

DAVIS

Approved:

_____
Tonya Kuhl, Chair

_____
Roland Faller

_____
Mark Asta

Committee in Charge

2012

ProQuest LLC.
789 East Eisenhower Parkway
P.O. Box 1346
Ann Arbor, MI 48106 - 1346

Dedicated to my father Mao-Yuan Liao and my mother Wei-Ming Lu.
To my wife Pei-Shan Yuan and my son Aaron Liao.

TABLE OF CONTENTS

Abstract

Polymer brushes, in particular, are formed when long-chain polymer molecules are attached at one end to an interface. When the spacing between attachment points is less than the polymer chain's radius of gyration, R_g, the chains overlap and are forced to stretch away from their attachment points to decrease crowding. This stretching along the direction normal to the grafting surface is different from the typical behaviors of flexible polymer chains in a solution and with wide application potential for modifying interfacial properties such as wetting, adhesion and lubrication. The stability or durability of the polymer brush layer was directly influenced by the surface coverage which will constrain the practical application. In standard grafting-to methods, the polymers were grafted on the surfaces by physical adsorption or covalent bonding of end-tailed functional group and the coverage is limited by the steric obstacle of the polymer itself during the process. In this work the force profiles of a series of moderate to high grafting density diblock copolymer brushes prepared by the spin-coating method are reported. Instead of accessing different grafting density regimes by changing the molecular weight (MW) of the blocks, a single diblock was used. Two distinct compression regimes were observed. The measured force profiles demonstrate scaling behavior and discrepancies between the experimental data and theory are discussed. To further explore the interactions between more highly-stretched brushes, the neutral Polystyrene (PS) films prepared by grafting-from method was also studied using surface force apparatus (SFA). Both the normal and shear force behaviors of the opposing ATRP-formed brushes are presented. Excellent lubricant performance was also observed.

Curriculum Vitae

Wei-Po Liao

Education

Ph.D. Candidate. Materials Science & Engineering, University of California-Davis

Designated Emphasis in Polymer Science

M.S. Chemical Engineering, National Cheng Kung University - Taiwan, 2002

B.S. Chemical Engineering, National Chung Hsing University - Taiwan, 2000

Honors & Awards

- Travel support program award by the National Science Foundation through the NIST/NSF Center for High Resolution Neutron Scattering (CHRNS), 2009

- Graduate Researcher/ Teaching Assistant Fellowship, Department of Chemical Engineering & Materials Science, University of California, Davis, 2007

Journal Publications & Presentations

1. ***Wei-Po Liao***, Ian Elliott, Tonya Kuhl. "Normal and Shear Interactions between High Grafting Density Polymer Brushes Grown by Atom Transfer Radical Polymerization", *submitted to Soft Matter* (in press).

2. ***Wei-Po Liao***, Tonya Kuhl. "Steric Forces of Tethered Polymer Chains as a Function of Grafting Density: Studies with a Single Di-Block Molecular weight", *Macromolecules*, 2012, 45, (14), 5766-5772

3. Chi Wang, ***Wei-Po Liao***, Ming-Ling Wang, Chang-Chun Lin. "Miscible Blends of Syndiotactic Polystyrene and Atactic Polystyrene. Part 2. Depolarized Light Scattering Studies and Crystal Growth Rates", *Polymer*, 2004, 45:973-981

4. Chi Wang, ***Wei-Po Liao***, Yong-Wen Cheng, Tsang-Lang Lin. "Miscible Blends of Syndiotactic Polystyrene and Atactic Polystyrene. Part 1. Lamellar Morphologies and Diluent Segregation", *Polymer*, 2004, 45:961-971

5. Chi Wang, ***Wei-Po Liao***, Yong-Wen Cheng. "Strong Diffuse Scattering and Lamellar Morphologies of Syndiotactic Polystyrene Polymorphic Effects", *Journal of Polymer Science: Part B: Polymer Physics*, 2003, Vol.41, 2457-2469

6. Chi Wang, Chao-Chen Chen, Yong-Wen Cheng, ***Wei-Po Liao***, Min-Ling Wang. "Simultaneous Presence of Positive and Negative Spherulites in Syndiotactic Polystyrene and Its Blends with Atactic Polystyrene", *Polymer*, 2002, 43:5271-5279

7. ***Wei-Po Liao,*** Tsang-Lang Lin, E. M. Woo, Chi Wang. "Lamellar Thickness of a Syndiotactic Polystyrene Determined from Small-angle X-ray Scattering and Transmission Electron Microscopy", *Journal of Polymer Research*, 2002, 9: 91-96

8. ***Wei-Po Liao,*** Yong-Wen Cheng, Ming-Ling Wang, Chi Wang. "The Morphological Lamella Structure of Syndiotactic Polystyrene when Blending with Atatic Polystyrene", 2002 *Annual ROC Polymer Symposium*, Taichung, Taiwan

9. ***Wei-Po Liao***, "Determination of Polymeric Microstructure by Small-angle Scattering", National Cheng Kung University, 2002

Acknowledgements

First, I would like to express my utmost gratitude to my advisor, Professor Tonya Kuhl, for her continuous and patient guidance. This dissertation would not have been possible without her constant encouragement and valuable discussions. The knowledge I have learned from her will be a cherishable asset for me not only in academia but also for my life in the future. It was the greatest honor and luck of mine to work with her. I wish to thank my committee members, Professor Roland Faller and Professor Mark Asta, for their advice and input to this dissertation.

Feedback and comments from the members of "Surface and Interfacial Science Laboratory" at UC Davis, Department of chemical Engineer and Materials Science have been enormously helpful to my projects, especially Dennis Mulder, Ian Elliott and Raquel Orozco-Alcaraz. I would also like to express my appreciation to Dr. Jarek Majewski at Lujan Neutron Scattering Center, Los Alamos National laboratory who provided technical instrument support. Those who have devoted substantial amount of time towards to the completion of this work are respectfully acknowledged.

Lastly and the most importantly, I would like to dedicate this achievement to my father Mao-Yuan Liao, my mother Wei-Ming Lu, my sister He-Ting Liao, my wife Pei-Shan Yuan and all the other family members for their understanding, wonderful support and everlasting love.

Overview

Chapter 1 describes the scope of the project. The main concepts about polymer brushes and relevant theory are discussed. The pros and cons between two major types of approaches to form polymer brushes are compared. The introduction also includes the potential applications as well as motivation for the studied systems. In addition, the instrumentation used to accomplish the projects is also briefly mentioned in the first chapter and is further discussed through data analysis in the following chapters. **Chapter 2** demonstrates systematic studies of high grafting density brushes achieved by a modified form of the generally studied "grafting-to" approach involving spin-coating of diblock polymer chains. The steric forces between opposing brush layers as a function of grafting density were measured using an automated Surface Force Apparatus. Different normalization means were applied on the profiles and universal force behaviors of the system is established. **Chapter 3** reports both the normal and shear interfacial interactions in good solvent conditions between two opposing ultra-high grafting density polymer brushes formed by atom transfer radical polymerization. A much higher grafting density compared to the conventional “grafting-to” was accomplished using this synthesis method. The steric force profiles of similar MW brushes formed by both “grafting-to” and “grafting-from” methods are compared. Within the experimental time scale, significant hysteresis is observed in the ultra-high grafting density brushes, demonstrating a much longer relaxation time for these conditions. The shear performance of the ultra-high density brushes demonstrates excellent lubrication and wear, comparable to lower grafting density brushes where hysteresis is not observed.

Chapter 4 provides additional characterization measurements and a proposed device for future advancements.

All the references and appendices referred to are listed at the end of each chapter.

Chapter 1: Introduction

Polymer brushes are created when at least one end of the polymer chain is tethered to a surface or interface. Tethering to the surface or interface is typically accomplished by physical adsorption or covalent bond.[1] The movements of the polymer chains are limited and restricted due to the confined environment and result in very different responses or behaviors compared to the freely moving polymer chains in a melt or solution. These differences make it possible for polymer brushes to be applied to many fields in surface modifications, such as wetting, adhesives, stabilizers or lubricants etc. My research topic is mainly focusing on polymers on flat surfaces and the following text will specifically discuss this. For polymer chains on flat surfaces, three different types of geometries are found.[2] When all or most of the polymer chains are adsorbed or attached on the surface, the flat distribution of the polymer takes the form of a pancake like geometry. Unlike the pancake geometry, if only one end of the polymer chain has affinity to the surface while rest of the chains want to dangle away from the surfaces into a medium, a mushroom structure of the polymer is formed. In this case, the size of the freely relaxed chain is equal to the radius of gyration (R_g) of the chain with the same molecular weight in the solution. The main criterion for a real brush-like geometry to form is to have enough polymer surface coverage. When increasing the amount of polymer on the surfaces, once the distance between the attached points of two adjacent polymers chain is smaller than the radius of gyration, the polymer chains will begin to

feel pressure and are forced to stretch away from the surface to form a brush-like structure. The extent of "stretching" will reach an equilibrium length. The most well-known Alexander-de Gennes Model [3-5] has predicted this equilibrium length using two approaches: Flory argument and scaling analysis. The concept of the Flory argument suggests the energy per chain could be described by two terms, osmotic pressure and elastic energy of the chain. The equilibrium length will be achieved when the free energy is a minimum. A blob model is assumed in the scaling method where the blob size is equal to the distance between grafting points. The dependence of the equilibrium length can be established after a series of scaling calculations. Both approaches give the same result: $L \sim aN\sigma^{1/3}$ where "L" is the equilibrium length; "a" is the monomer size; "N" is the degree of polymerization; "σ" has the unit of chains per unit area.

Table 1. The assumptions from three different theoretical models for polymer brushes. [3, 4, 6-10]

	Alexander-de Gennes (Alexander, 1977; de Gennes 1980)	ASCF (Milner,1988)	NSCF (Whitmore,1990,2005)
Density profile	Step like	• Maximum at the surface • Parabolic-good solvent • Elliptical-theta solvent	Rises smoothly from surface to a maximum and then decreases smoothly and monotonically to zero, ending in an extended tail
Depletion layer	Allows a depletion layer	No depletion layer	No assumption
Mechanism	• Neutral surface • No difference between repulsive, attractive or neutral surfaces		Can discriminate among mechanisms
Interpenetration	Merely compression	No interpenetration	Allows interpenetration

The A-dG model provides a useful and straightforward method to predict the behavior of polymer brush systems. More recent theoretical and simulation work [9, 11, 12] has been carried out to modify and improve upon the assumptions of the A-dG model and will be further discussed in the following chapters. The key assumptions from three different theoretical models are summarized in Table 1. For the systems I focus on in my research work, most of the experimental data was compared with both the A-dG and the Milner-Witten-Cates (MWC) models.

Polymer brush systems are flexibile and efficient means for surface modification and tailoring for a broad array of applications. For example, the principle of "Smart surfaces" is to change the properties of the surfaces by coating or grafting varied types of polymers that are responsive to different external stimuli, such as temperature, pH value, electrolyte and solvent quality. [13-16] The ability to tailor surface properties has opened up even more potential applications for the use of polymer brushes as the surface properties can be manipulated by different control parameters. Another fascinating application of polymer brush coatings that is particularly attractive to me is the ability to form an extra-low friction coefficient films even under high load. Back in the 1990s, Klein et al.[17] performed a set of experiments to measure both the normal and shear force between opposing polystyrene brush layers in toluene and found out that the combination of polymer brushes in good solvent could effectively reduce the friction coefficient at the sliding interface. The mechanism for friction reduction was thought to be very similar to the human joint system. Subsequently, a large body of work has been devoted to obtaining a better understanding of the shear performance of different brush systems as a function of solvent conditions and confinement.[18-22] This work is

focused on both the shear and normal interactions of polymer brushes formed by two different approaches in order to obtain a range of grafting densites. The systematic study of their properties contributes to the fundamental understanding of the physics and design of polymer brushes that have not previously been discussed or observed.

In addition to the force studies, the surface structure information of the brushes has also been extracted in the project discussed in the following chapters to establish the structure-property correlation. The main instruments chosen to accomplish the interaction and structure measurements are the surface force apparatus (SFA) and neutron reflectivity technique (NR).

The SFA was first developed to measure the van der Waals forces between surfaces in air in the distance regime of 1.5-130 nm in 1969, by Tabor and Winterton[23] and later improved upon in 1972, by Israelachvili and Tabor[24]. Based on the successful measurements using this powerful tool, a number of different versions have been extensively discussed and modified.[25-31] The model that has been utilized in this project is an "Israelachvili type" Mark II SFA, a stainless box with approximately 340 mL in volume (Figure 1).

The SFA measures the force-distance profile between two cross cylinder mica sheets supported on glass disks of ~1.5 cm radius of curvature. Forces are obtained by the displacement of weak double cantilever spring mounted to one of the surfaces while the distance between the two surfaces is measured directly by utilizing white-light interferometry that gives rise to fringes of equal chromatic order (FECO). The theoretical resolution is about 10^{-8} N in force and about 1Å in distance.

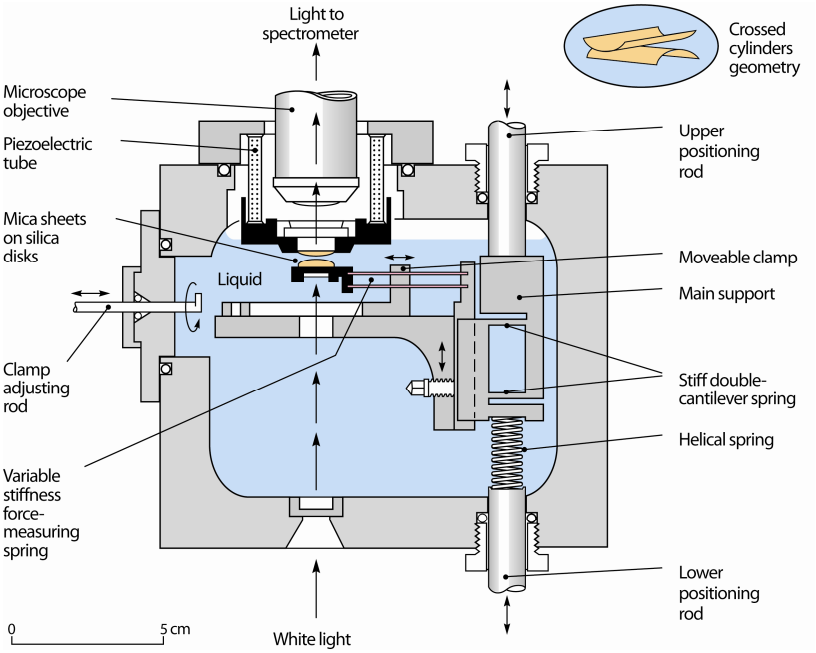

Figure 1. Schematic of Mark II surface force apparatus (SFA).

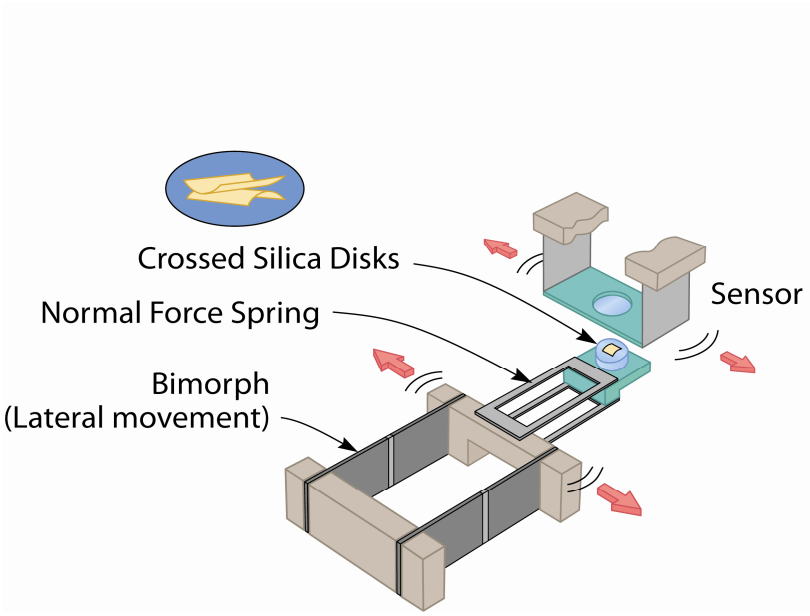

Figure 2. Schematic of the friction force attachment.[32]

In addition to the normal force, the shear interaction can also be measured using an SFA with an additional attachment. Both the top and lower sample mounts can be replaced by the friction attachment as shown in Figure 2.[32] The main point of the device is the bimorph slider which is assembled by combining two piezoelectric sheets with reversed polarity. When a voltage is applied, one piezoelectric sheet in the bimorph assembly contracts while the other sheet expands. The combined response of the both bimorphs to the applied voltage makes parallel lateral movement possible. The top surface is mounted in a "receiver", which has vertical springs to act as a sensor to detect the lateral shear forces transmitted through the interface between two opposing polymer brushes.

The interface interaction measurement can also be achieved by other instruments that operate microscopically or macroscopically. For example, the surface forces between two opposing end-grafted poly(methyl methacrylate) (PMMA) brushes have been studied with atomic force microscopy (AFM),[33] while the macroscopic shear performance have been examined on poly 2-methacryloyloxyethyl phosphorylcholine (Poly(MPC)) brushes using the conventional ball-on-disk tribometer.[34] However, neither the AFM or ball-on-disk tribometer can extract force-distance information of the normal and lateral shear forces acting between surfaces as precisely as the SFA. The SFA provides both a direct measurement of the surface separation and any surface deformation with a well-characterized area of contact with high resolution in distance and force. Such capabilities are very advantageous when studying polymer brush systems.

The neutron reflectivity (NR) technique was used to conduct complementary measurements of polymer brush structure. NR provides details of the thin polymer film

structure such as thickness, roughness, uniformity, and density profile of the layers normal to the interface or surface with sub-nanometer resolution.[35] Additional features of these measurements are the ability to probe buried interfaces due to the high penetration of neutrons through thick samples, contrast matching techniques and/or deuterium labeling to highlight or mask certain portions of the samples, with negligible radiation damage. Most of the neutron measurements presented in this work were carried out on the SPEAR reflectometer at the Manuel Lujan Jr. Neutron Scattering Center at Los Alamos National Laboratory.[36] Further details of the instrument and fitting process are provided in ref. 36. Details regarding the analysis methods and the experimental concepts will be discussed in the following chapters.

As described previously, polymer brush systems have various applications in many different fields. Klein et al. have shown potential of polymer brushes to minimize the shear interaction between sliding surfaces, which demonstrates their great possibility to act as lubricating layers under high load.[17] Since those pioneering studies, polymer brushes in good solvent condition have been proven to effectively decrease the friction coefficient compared to simply sliding surfaces in the bulk solvent. [17-20, 37] Subsequently, charged polyelectrolyte brushes have been reported to have even better frictional behavior compared to neutral brushes.[38-40] Methods for preparing polymer brushes can be separated into two categories: the “grafting-to” and “grafting-from” Methods. The main difference between the two approaches is whether the polymer brush layer is formed after the polymer is fully synthesized or not. For the “grafting-to” approach, the fully-synthesized polymer is tethered on a surface or an interface by preferential physical adsorption of an amphiphilic block copolymer in the selective

solvent or by the physisorption or covalent bonding between an end-tailored functional group of the polymer chain and the substrate. In the "grafting-from" case, the polymer is grown directly from the surface monomer by monomer and the thickness of the film is controlled by the polymerization time. Due to steric obstacle effects between the polymer chains, the amount of polymer on the surface by using the "grafting-to" method is not as much as the "grafting-from" method where the size of a monomer is substantially smaller than the polymer chain. In this work, a novel means to increase the amount of polymer on the surface beyond that typically obtained in a "grafting to" method was employed. Here, spin-coating from solution was utilized to substantially increase the surface coverage of a "grafted to" brush. Details of this approach will be discussed in the following chapter. In follow on work, the grafting-from approach was used to access even denser polymer brush films. In addition, a further benefit of the "grafting from" approach is that the polymer brush is covalently bonded to the surface. Thus, these brushes provide a more durable layer to meet realistic application requirements. Moreover, the synthesis method used in the grafting-from approach increases the flexibility in materials selection through the length of the polymer chain and enables more complex chain compositions and architectures to be assessed. The SFA technique is one of the most powerful means to study both the normal and lateral interaction as a function of separation of the opposing polymer brushes. In this work, SFA measurements are used to establish the correlation between the various brush parameters and their normal and shear interaction properties. However, the substrate normally used for SFA is mica due to its molecularly smooth surface. Mica is not a practical surface for "grafting from" systems as it is chemically inert. Moreover, it is

easily damaged and has a high surface adhesion. The most commonly used substrate for the polymerization methods such as "grafting from" is silica. Although mica (an alumina-silicate) does have some surface OH sites, their number is much less than that on silica surfaces. The amount of surface OH groups is the key for flexible surface reactivity and makes mica and silica significantly different in general. As a result, some modifications or substitutions for mica substrates commonly used in the SFA were carried out to accomplish this work.

In Ruth's SFA work,[41] mica was replaced with tube-blown glass to enable the reactivity for the "grafting from" method through living radical polymerization. Silica pieces a few micrometers in thickness were obtained and used as substrates for polymer synthesis. Within the measuring area of SFA ~30 x 30 μm^2, the roughness of the glass tube blown silica films was 0.5nm as measured by AFM. The uniformity in thickness of the silica piece was less controllable and more difficult to determine using this method. Thicker silica pieces not only decrease the resolution of the measurement but also affect the optics. Moreover, the asymmetric configuration of the silica surfaces increases the complexity of the data analysis. Lego et al. increased the number of OH groups on mica surfaces by using plasma discharge in water vapor. Lego et al. were then able to chemically bond initiators for the polymer synthesis reaction to the modified mica surface.[42] The thickness of the initiator layer was determined by the step-height measurement using AFM (0.7±0.1 nm). The number and the distribution of the activated sites on mica was obtained using time-of-flight secondary ion mass spectrometry (TOF SIMS) after the initiator were bonded on the surfaces. When increasing the plasma treatment time, more initiators were found and the results were consistent with the

measured increase in water contact angle. This surface modification strategy was also used by Dunlop et al. to grow polyelectrolyte layers from mica substrates.[38] In Vigil et al.'s work,[43] the interactions between a thin silica film deposited on mica surfaces were measured by SFA. Electron beam evaporation was used to deposit silica from quartz onto the mica surfaces. The roughness of the deposited silica layers was 3.7±0.5Å determined by AFM while the thickness and the refractive index were obtained from ellipsometry. The refractive index was comparable with the bulk silica. Based on their observation, hydrophilic silica layers was found to swell under humidity, and this swelling increased with the relative humidity. Under the thickness range of the deposited silica from 100Å to 1000Å, the swelling thickness was found to range from 2 to 20Å. No further swelling was observed between 100% relative humidity and immersion in bulk water. In all cases, the swelling ratio was less than 2% compared to the dry silica layer thickness. All of the strategies mentioned above are able to increase the reactivity of the surfaces to make living radical polymerization reactions feasible from the surface, the silica deposition method using electron beam (E-beam) was chosen for the presented work in the following chapters.

In order to apply polymer brushes to a lubricant system, one of the major concerns is the durability of the polymer film. One way to improve the polymer film's durability is to increase its surface coverage. In the next two chapters, polymer films with higher surface coverage are achieved by modifying the conventional grating-to method as well as taking advantages of the grafting-from method. The interfacial interactions between the opposing brushes formed by these two approaches have been studied systematically and the corresponding structures of the single surfaces both in air and solvated have also been

determined. The presented work in this thesis will provide information about how polymer brushes with intermediate to very high concentration behave and also demonstrate their potential in shear performance of ultra-high surface coverage polymer brushes.

References

1. Zhao, B. and W.J. Brittain, *Polymer brushes: surface-immobilized macromolecules.* Progress in Polymer Science, 2000. **25**(5): p. 677-710.
2. Advincula, R.C., et al., *Polymer Brushes:Synthesis, Characterization, Applications*2004: Wiley-VCH.
3. Alexander, S., *Adsorption of Chain Molecules with a Polar Head a-Scaling Description.* Journal De Physique, 1977. **38**(8): p. 983-987.
4. Alexander, S., *Polymer adsorption on small spheres: A scaling approach.* Journal de physique., 1977. **38**(8): p. 977-982.
5. de Gennes, P.G., *Conformations of Polymers Attached to an Interface.* Macromolecules, 1980. **13**(5): p. 1069-1075.
6. Milner, S.T., T.A. Witten, and M.E. Cates, Macromolecules, 1988. **21**: p. 2610.
7. Milner, S.T., T.A. Witten, and M.E. Cates, *Theory of the grafted polymer brush.* Macromolecules, 1988. **21**(8): p. 2610-2619.
8. Milner, S.T., *Compressing polymer brushes—a quantitative comparison of theory and experiment.* Europhysics Letters, 1988. **7**: p. 695-699.
9. Whitmore, M.D. and R. Baranowski, *End-anchored polymers: Compression by different mechanisms and interpenetration of apposing layers.* Macromolecular Theory and Simulations, 2005. **14**(2): p. 75-95.
10. Whitmore, M.D. and J. Noolandi, *Theory of adsorbed block copolymers.* Macromolecules, 1990. **23**(13): p. 3321-3339.

11. Milner, S.T., T.A. Witten, and M.E. Cates, *A Parabolic Density Profile for Grafted Polymers.* EPL (Europhysics Letters), 1988. **5**(5): p. 413-418.

12. Baranowski, R. and M.D. Whitmore, *Numerical self-consistent field study of tethered chains in Theta solvent.* The Journal of Chemical Physics, 1998. **108**(23): p. 9885-9892.

13. Minko, S., *Smart Responsive Coatings from Mixed Polymer Brushes*, in *Smart Coatings*2007, American Chemical Society. p. 79-93.

14. Sanjuan, S., et al., *Synthesis and Swelling Behavior of pH-Responsive Polybase Brushes.* Langmuir, 2007. **23**(10): p. 5769-5778.

15. Guo, Y. and M.G. Moffitt, *Semiconductor Quantum Dots with Environmentally Responsive Mixed Polystyrene/Poly(methyl methacrylate) Brush Layers.* Macromolecules, 2007. **40**(16): p. 5868-5878.

16. Yamamoto, S.-i., J. Pietrasik, and K. Matyjaszewski, *Temperature- and pH-Responsive Dense Copolymer Brushes Prepared by ATRP.* Macromolecules, 2008. **41**(19): p. 7013-7020.

17. Klein, J., et al., *Reduction of frictional forces between solid surfaces bearing polymer brushes.* Nature, 1994. **370**(6491): p. 634-636.

18. Forster, A.M., J.W. Mays, and S.M. Kilbey, *Effect of temperature on the frictional forces between polystyrene brushes.* Journal of Polymer Science Part B: Polymer Physics, 2006. **44**(4): p. 649-655.

19. Schorr, P.A., et al., *Shear Forces between Tethered Polymer Chains as a Function of Compression, Sliding Velocity, and Solvent Quality.* Macromolecules, 2003. **36**(2): p. 389-398.

20. Raviv, U., R. Tadmor, and J. Klein, *Shear and Frictional Interactions between Adsorbed Polymer Layers in a Good Solvent.* The Journal of Physical Chemistry B, 2001. **105**(34): p. 8125-8134.

21. Grest, G., *Normal and Shear Forces Between Polymer Brushes*, in *Polymers in Confined Environments*1999. p. 149-183.

22. Klein, J., et al., *Shear forces between sliding surfaces coated with polymer brushes: The high friction regime.* Acta Polymerica, 1998. **49**(10-11): p. 617-625.

23. Tabor, D. and R.H.S. Winterton, *The Direct Measurement of Normal and Retarded van der Waals Forces.* Proceedings of the Royal Society of London. Series A, 1969. **312**: p. 435-.

24. Israelachvili, J. and D. Tabor, *The Measurement of Van Der Waals Dispersion Forces in the Range 1.5 to 130 nm.* Proceedings of the Royal Society of London. Series A, 1972. **331**(1584): p. 19.

25. Israelachvili, J., *direct measurement of forces between surfaces in liquids at the molecular level.* Proc. Natl. Acad. Sci. USA, 1987. **84**: p. 4722-4724.

26. Klein, J., *Forces between mica surfaces bearing layers of adsorbed polystyrene in cyclohexane.* Nature, 1980. **288**(5788): p. 248-250.

27. Tonck, A., J.M. Georges, and J.L. Loubet, *Measurements of intermolecular forces and the rheology of dodecane between alumina surfaces.* Journal of Colloid and Interface Science, 1988. **126**(1): p. 150-163.

28. Parker, J.L., H.K. Christenson, and B.W. Ninham, *Device for measuring the force and separation between two surfaces down to molecular separations.* Review of Scientific Instruments, 1989. **60**(10): p. 3135-3138.

29. Israelachvili, J.N. and M. McGuiggan, *Adhesion and short-range forces between surfaces. Part I: New apparatus for surface force measurements.* J. Mater. Res., 1990. **5**.

30. Israelachvili, J.N. and G.E. Adams, *Direct measurement of long range forces between two mica surfaces in aqueous KNO3 solutions.* Nature, 1976. **262**(5571): p. 774-776.

31. Israelachvili, J.N. and G.E. Adams, *Measurement of forces between two mica surfaces in aqueous electrolyte solutions in the range 0–100 nm.* J. Chem. Soc., Faraday Trans., 1978. **1**(74): p. 975 - 1001.

32. Luengo, G., et al., *Thin Film Rheology and Tribology of Confined Polymer Melts: Contrasts with Bulk Properties.* Macromolecules, 1997. **30**(8): p. 2482-2494.

33. Yamamoto, S., et al., *Surface Interaction Forces of Well-Defined, High-Density Polymer Brushes Studied by Atomic Force Microscopy. 1. Effect of Chain Length.* Macromolecules, 2000. **33**(15): p. 5602-5607.

34. Kobayashi, M., et al., *Friction behavior of high-density poly(2-methacryloyloxyethyl phosphorylcholine) brush in aqueous media.* Soft Matter, 2007. **3**(6): p. 740-746.

35. Russell, T.P., *X-ray and neutron reflectivity for the investigation of polymers.* Materials Science Reports, 1990. **5**(4): p. 171-271.

36. Dubey, M., et al., *SPEAR — ToF neutron reflectometer at the Los Alamos Neutron Science Center.* The European Physical Journal Plus, 2011. **126**(11): p. 1-11.

37. Klein, J., et al., *Lubrication forces between surfaces bearing polymer brushes.* Macromolecules, 1993. **26**(21): p. 5552-5560.

38. Dunlop, I.E., et al., *Direct Measurement of Normal and Shear Forces between Surface-Grown Polyelectrolyte Layers†.* The Journal of Physical Chemistry B, 2009. **113**(12): p. 3947-3956.

39. Briscoe, W.H., et al., *Boundary lubrication under water.* Nature, 2006. **444**(7116): p. 191-194.

40. Raviv, U. and J. Klein, *Fluidity of Bound Hydration Layers.* Science, 2002. **297**(5586): p. 1540-1543.

41. Ruths, M., et al., *Repulsive Forces and Relaxation on Compression of Entangled, Polydisperse Polystyrene Brushes.* Macromolecules, 2000. **33**(10): p. 3860-3870.

42. Lego, B., W.G. Skene, and S. Giasson, *Unprecedented Covalently Attached ATRP Initiator onto OH-Functionalized Mica Surfaces.* Langmuir, 2007. **24**(2): p. 379-382.

43. Vigil, G., et al., *Interactions of Silica Surfaces.* Journal of Colloid and Interface Science, 1994. **165**(2): p. 367-385.

Chapter 2: Steric Forces of Tethered Polymer Chains as a Function of Grafting Density: Studies with a Single Di-Block Molecular Weight

2.1 Abstract:

The normal force to compress opposing polymer brushes as a function of grafting density was measured using a surface force apparatus. In contrast to conventional methods where grafting density has been varied by changing polymer molecular weight, in this work high grafting densities ranging from 1.4 to 7.6 mg/m^2 were obtained by spin coating different concentrations of a single diblock copolymer. Measured force profiles at low grafting density, σ <4 mg/m^2, were analogous to previous studies and consistent with Milner-Witten-Cates (MWC) theoretical predictions once chain polydispersity was accounted for. At higher grafting densities the experimentally measured repulsive interaction energy or force showed scaling behavior where the non-dimensionalized force curves fall on top of each other; however the behavior is distinctly different from the low grafting density regime and cannot be modeled using theory developed for the dilute/semi dilute regime.

2.2 Introduction

Surface grafted polymers layers are widely used to modify interfacial properties such as wetting, adhesion and lubrication[1-3]. Polymer brushes, in particular, are formed when long-chain polymer molecules are attached at one end to a surface. When the spacing between attachment points is less than the polymer chain's radius of gyration, R_g, the chains overlap and are forced to stretch away from their attachment points to decrease crowding. This stretching along the direction normal to the grafting surface is different from the typical behaviors of flexible polymer chains in a solution [4]. The resulting brush structure depends intimately on the chain molecular weight, grafting density, and solvent quality [5]. Because of their wide application, a large body of experimental [6-16], theoretical [4, 17-23] and simulation work [24-30] has been carried out in order to characterize and ultimately predict the properties of polymer brushes. However, polymer brushes with high grafting densities have not been studied extensively due to experimental limitations when forming brushes; theoretical challenges in handling highly interacting systems, and computational limitations in simulating long chain systems.

In the standard "grafting-to" method, the brush layers are prepared by physical adsorption where the surface coverage depends on the polymer-surface-solvent interaction, but is limited by the steric obstacle of the polymer itself during the adsorption process. The dimensionless overlap surface density, Σ, is defined as $\Sigma=\sigma\pi R_g^2$, where σ is the experimental chain grafting density (chains/Å^2), and R_g is the radius of gyration of a free polymer chain in solution[26]. Thus, the chains start to overlap and interact when $\Sigma\geq 1$, and become more stretched as surface coverage increases. In this work, high coverages

or grafting densities were obtained by spin-coating and annealing polymer diblocks of polystyrene-polyvinyl pyridine (PS-P2VP). In a selective solvent such as toluene, the PS layer forms a brush while the P2VP anchors the PS brush to the underlying substrate. The PS-P2VP system has been studied extensively in both good and theta solvent conditions. For example, the extension and compression of comparable molecular weight (MW) to that studied here has been measured using both the surface force apparatus and atomic force microscopy, but only for relatively low grafting densities, $\Sigma \leq 5$, [7, 14, 31-34]. For higher grafting densities, Kent and coworkers have carried out and analyzed neutron reflectivity experiments to extract the structure of polymer brushes formed as Langmuir monolayers from polydimethylsiloxane-polystyrene diblocks at the air/ethyl benzoate interface [35, 36]. The highest reduced grafting density with similar MW was 9.9, and a comprehensive comparison of brush height and density of a single brush layer was made. More recently the grafting-from approach, where the polymer brush layer is polymerized in-situ from surface tethered initiator molecules, has been used to generate ultra-high grafting densities[3, 5, 12, 37, 38]. For example, Ruths et al. achieved a grafting density, $\Sigma \geq 56$, with very high MW polystyrene chains using the grafting from approach. However, explicit comparison of the measured force profiles to theory was hampered by the large chain polydispersity, PDI$\geq$1.6. In contrast to physical experiments, numerical studies can more easily probe high grafting densities in a controlled manner. For instance, a detailed appraisal of brush structure and compression for a wide range of grafting densities has been done by Whitmore and coworkers[27, 39] using self-consistent field theory. Coarse grained molecular dynamics simulations are also beginning to explore the high density regime[30]. However, experimental steric force

measurements with strongly stretched brushes, $\Sigma \geq 10$, formed by grafting-to method have not yet been systematically studied. In this work the force profiles of a series of moderate to high grafting density diblock copolymer brushes are reported. Instead of accessing different grafting density regimes by changing the MW of the blocks, a single diblock was used. Two distinct compression regimes were observed; one for moderate grafting densities, $\Sigma \leq 5$, and the other for $\Sigma > 10$. The measured force profiles demonstrate scaling behavior and discrepancies between the experimental data and theory are discussed.

2.3 Experimental Section

2.3.1 Polymer Film Preparation:

A 50:50 polystyrene-b-poly-(2-vinylpyridine) (PS-P2VP) diblock copolymer with molecular weight 1.14 x 10^5 g/mol and 1.08 polydispersity index (PDI) from Polymer Source (Quebec, Canada) was used for these studies. Polymer film preparation was based on procedures developed for creating high density brushes on hydrophilic surfaces for neutron reflectivity studies[13, 40, 41]. The desired concentration (0.3-1.0 % g/mL) was made by dissolving the polymer in toluene with continuous stirring for at least 24 hours. Just prior to use, the solution was filtered a minimum of 2 times and 1 time through 0.45μm and 0.2μm PTFE filters sequentially. Uniform polymer films were then deposited on the desired surface by spin coating at 2000 rpm for 30 seconds. For neutron reflectivity measurements, uv-ozone cleaned silicon or quartz substrates were used. For SFA experiments, ~4 micron thick, molecularly smooth mica sheets were used. The mica

pieces were cleaved to the desired thickness and placed on a freshly cleaved mica backing sheet. After spin-coating, the deposited film was annealed under vacuum at 180°C for 48 hours. The glass transition temperature for both polymers is about 100°C. The P2VP prefers to wet hydrophilic (oxide) surfaces while PS segregates to the air interface[13, 41, 42]. After annealing, an equilibrium alignment of lamellae parallel to the substrate is obtained due to preferential surface wetting and the incompatibility of the PS and P2VP blocks. For SFA experiments, after annealing the mica surfaces with polymer film were flipped, placed on another mica backing sheet, and a ~550Å silver layer was deposited on the other side. The coated mica surfaces were then glued, silver side down, on to cylindrically curved glass disks using a 50:50 mixture of dextrose and D-galactose sugar glue. Neutron reflectivity measurements simply used the annealed films.

2.3.2 Neutron Reflectivity Measurements of Polymer Films in Air.

The structure of the annealed PS-P2VP films was verified using neutron reflectivity on the SPEAR reflectometer at the Manual Lujan Jr. Neutron Scattering Center at Los Alamos National Laboratory. Details of the instrument[43], measurement technique[44, 45] and fitting[13] have been previously described. Briefly, specular reflectivity measured as a function of momentum transfer, $Q_Z = (4\pi \sin\theta)/\lambda$, provides information on the in-plane average coherent scattering length density (SLD) profile and can be used to determine the concentration of atomic species at a particular depth in the material. Visible fringes in the reflectivity profile arise from interference between waves being

reflected from the different interfaces in the sample. From the measured reflectivity profile, the SLD, thickness, and roughness of the layers can be determined by modeling the SLD profile and iterating to minimize the difference between the measured reflectivity profile and that obtained from the modeled SLD profile.

Figure 1a shows the measured reflectivity profiles of spin-coated and annealed PS-P2VP layers in air. The data were fit with the MOTOFIT reflectivity analysis package and nonlinear least-squares regression[46]. For the simple case of a PS-P2VP film in air, boxes of constant thickness and SLD were used to model the PS and P2VP portion of the thin-film polymer layer. Interfaces were smeared with an error function. The inset shows the SLD of the corresponding line fit to the data. Well segregated layers of PS and P2VP were observed for concentrations below 1.0% by weight, consistent with previous literature[13, 41]. The larger roughness of the thickest film (~400Å) is likely due to the formation of small islands on the surfaces due to the film thickness exceeding the maximum for single lamellae at this concentration. A graph of the experimental air thickness as a function of spin coating solution concentration is shown in Figure 1b.

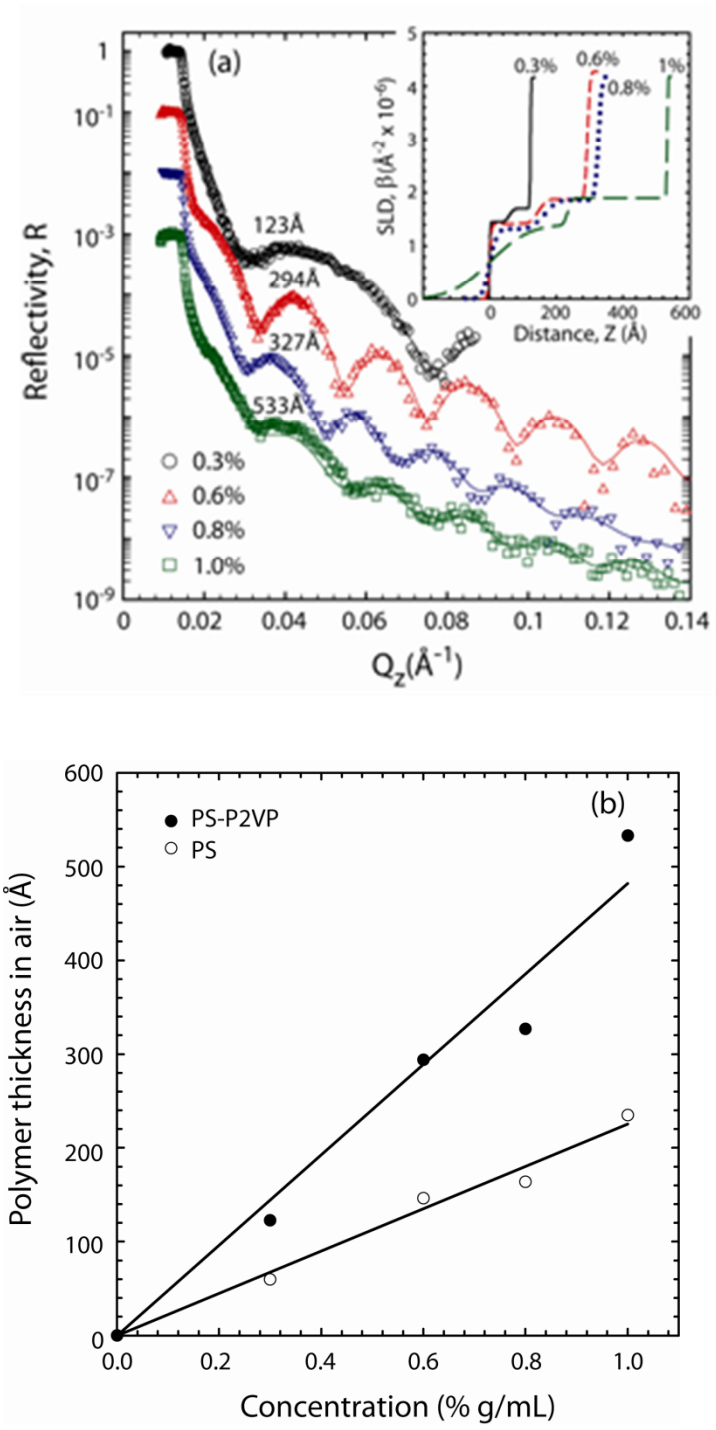

Figure 1. (a) Measured neutron reflectivity profiles and scattering length density fit for four different polymer film thicknesses in air. Profiles are shifted by an order of magnitude for clarity. (Inset) Corresponding neutron scattering length density profiles of the line fits to the data. (**b)** Comparison of the total polymer film thickness and PS portion from NR measurements as a function of spin-coating solution concentration.

2.3.3 Force-Distance Measurements.

The surface forces apparatus (SFA) technique has been previously described and has been used extensively to measure interaction forces between surfaces[47-49]. A Mark II SFA was utilized in this study and measurements were conducted at 25±0.2°C. The measured radius of curvature for each contact position was used to normalize the measured force profile to enable quantitative comparison between different contact positions and experiments. The Derjaguin approximation[50] gives the relationship between the interaction energy per unit area, *E*, for two flat plates from the measured force-distance, *F (D)*, relationship between two crossed cylinders

$$E(D) = \frac{F(D)}{2\pi R} \tag{1}$$

The Derjaguin approximation is valid at small distances where $D << R$. The radius of curvature was measured for two cross sections, at 90º and the geometrical mean was used in calculations. For these experiments the measured radius of curvature was 1.2 ± 0.25 cm.

Before measurements with PS-P2VP coated mica, contact between bare mica plates was established using mica substrates of the same thickness as those with the annealed polymer film. Next, contacts of the dry, annealed polymer films were measured at different locations on the surfaces to determine the uniformity of the deposited film. From the contact wavelength difference of the fringes of equal chromatic order (FECO) of the bare and polymer coated mica, the dry film thickness was determined[47]. Subsequently, the surfaces were separated a couple of millimeters and the SFA was filled

with toluene. The surfaces were brought close together and the film was left solvating for 24 hours before measuring the force profile. Multiple contact positions were measured and at least 3 approach and separation cycles were recorded for each position. The polymer layers were allowed 1 to 2 hours to relax after each cycle and no hysteresis was observed.

In contrast to adsorbed polymer brushes formed in-situ from submicellar polymer concentrations, an important consideration for these measurements was to define the "zero" distance and corresponding thickness of the solvated polymer brush. Compared to the measurements in air, up to half of the dry film thickness was lost upon solvation with toluene. The loss of material was relatively uniform as very similar solvated thicknesses were obtained from different contact positions over the course of an experiment. This indicated that any polymer desorption occurred upon exposure to the solvent-air interface, and was homogeneous rather than regional. The polymer thickness was, therefore, based on hard contact of the solvated film, and the grafting density was calculated accordingly. This method was verified to be a reasonable assumption by measuring the dry polymer thickness in air at the same contact location after the film was highly compressed and dried in vacuum for more than two days. After drying less than 3 percent difference in the thickness compared with the highly compressed solvated film was found. The P2VP thickness was assumed to be half of the total dry thickness of the polymer layer at contact based on the 50:50 diblock ratio and the poor swellability of P2VP in toluene[7, 14]. Moreover, any error from neglecting the swelling of P2VP in toluene is negligible compared to the extension of the PS brushes. For ease of comparison between the various grafting densities, the distance, D, utilized in the force profiles was defined as the

distance between two PS/P2VP interfaces. In other words, *D* represents the thickness or extension of the polystyrene brushes only. We finally note that the grafting densities of the spin-coated polymer brushes studied here were significantly higher than the submicellular polymer solution adsorption methods used previously.

2.3.4 Neutron Reflectivity Measurements of Solvated Polymer Films.

Some removal of the polymer film upon solvation with deuterated toluene was also observed via neutron reflectivity measurements. In modeling the solvated reflectivity profile, we assumed that a uniform film was still obtained as observed in the SFA experiments. For uniformly grafted polymer brushes in good solvent, both theory and simulations predict a parabolic density profile away from the surface followed by a long decaying tail. The reflectivity profile of solvated PS-P2VP brush that matches the high grafting density regime in the SFA experiments is shown in Figure 2a. To better demonstrate the quality of the fit, the data is plotted as RQ^4. The neutron reflectivity data was fitted using the MIRROR program developed by Hamilton, which is based on the iterative, dynamical method[51]. The MIRROR program calculates reflectivity using the optical matrix method from boxes of constant thickness and scattering length density. The SLD model used to fit the data is based on a power law curve extending from the P2VP layer with an exponentially decaying polymer tail region extending into the solvent. More details have been explicitly discussed in reference 13. The corresponding scattering length density (SLD) profile of the fitted model is shown in Figure 2b.

The SLD profile (figure 2b) was converted to volume fraction of polystyrene using:

$$SLD_{fitted} = \phi_{PS}(SLD_{PS}) + (1-\phi_{PS})SLD_{toluene} \quad (2)$$

Figure 2c plots the volume fraction profile of the solvated brushes and shows a power law fit to the data:

$$\phi(z) = \phi_0\left[1-(z/h_0)^n\right] \quad (3)$$

where φ_0 is the volume fraction of the polymer brush at the surface and h_0 is the unperturbed extension of the brush. The exponential decaying tail was modeled using $\phi(z) = \phi_t \exp(\frac{-z}{h_t})$ where h_t and φ_t are fitted values[16]. The surface density of the brush was determined by integrating the volume fraction profile (Figure 2c) yielding Σ=16.0. The PS brush extension of ~550Å matches well to the onset of repulsive force between brushes at the highest concentration studied in the SFA experiments (discussed in the following section). Due to a difference in the amount of polymer removed upon solvating the films on quartz and mica with toluene and deuterated toluene, respectively, we were unable to match neutron reflectivity measurements to the other grafting densities studied in the SFA.

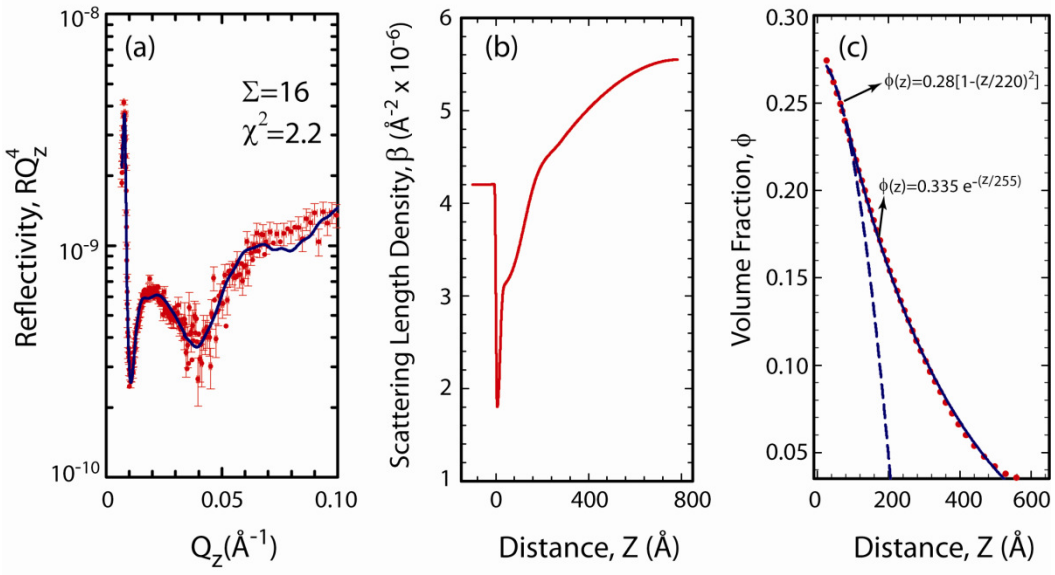

Figure 2. (a) Neutron reflectivity profile and fit for a solvated PS-P2VP brush in toluene with an overlap surface density, Σ=16. **(b)** Fitted scattering length density profile corresponding to the fitted line through the data in **(a). (c)** Volume fraction profile of the solvated PS brush layer.

2.4 Results and Discussion

The force profiles for five different brush grafting densities were measured using the SFA. The different conditions are reported based on their dimensionless surface density, Σ, which ranged from 3.0 to 15.8 based on the measured polymer thickness (Experimental Section). As can be seen in Figure 3, in all cases the measured interaction is purely repulsive between opposing polystyrene brush layers in good solvent conditions. With increasing grafting density, the magnitude of the normal force and distance of the onset of the repulsion increased. For comparison, $2h_{exp}$, which is defined as the onset of the repulsion between the symmetric brushes, is also indicated by arrows in Figure 3. There is excellent agreement between the brush extension measured with the SFA for Σ=15.8 and that measured for a single brush at the solid solution interface by neutron reflectivity,

Σ=16.0. Relevant experimental parameters of the various polymer brushes are summarized in Table 1. The total polymer thickness and error were determined from the average thickness measurements from different experiments and compression cycles. The PS grafting density was obtained from the measured thickness and the block copolymer ratio. The measured brush extensions from Figure 3 are also provided.

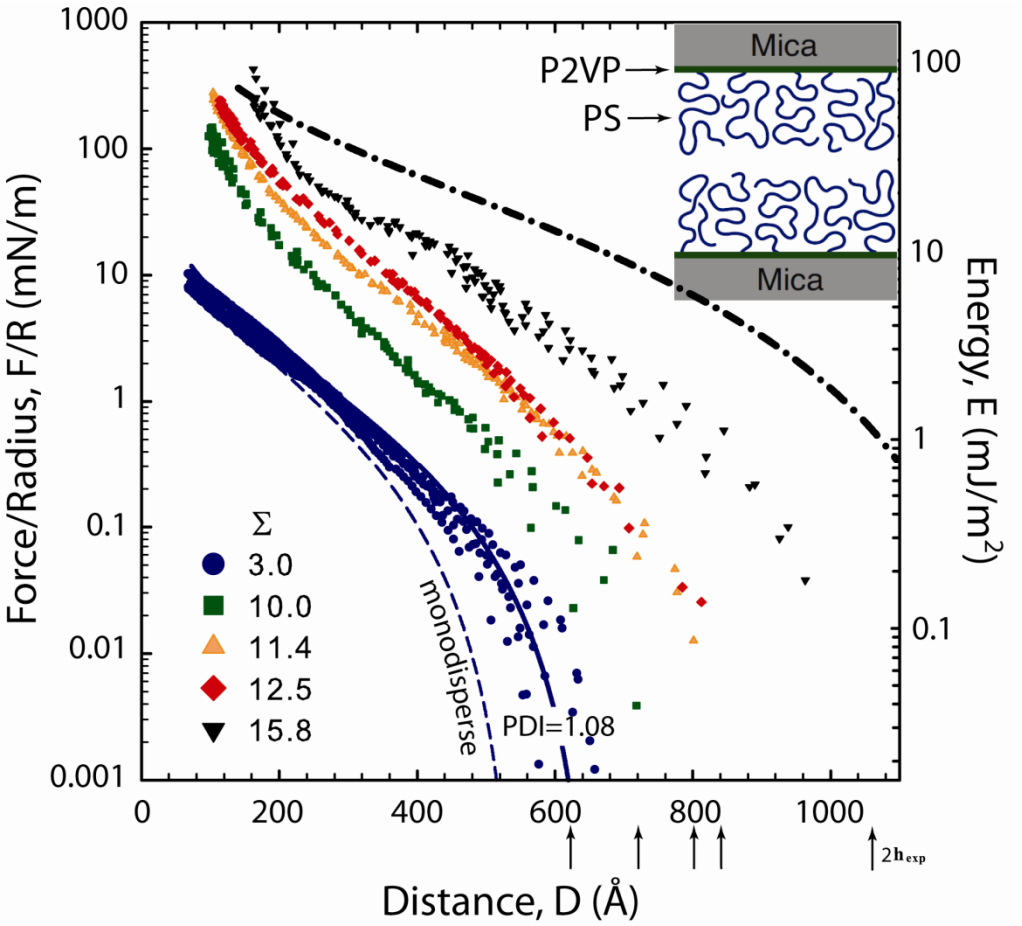

Figure 3. Measured normal force profiles of PS brushes for five different grafting densities. Arrows depict the onset of the repulsion for each grafting density. The right axis shows the corresponding interaction energy per unit area for flat surfaces. For overlap surface density, Σ=3, the dashed and solid curves show the Milner, Witten, and Cates (MWC) prediction for a mono-disperse and poly-disperse brush (PDI=1.08), respectively. The dash-dotted line shows the MWC prediction with a PDI=1.08 for Σ=15.8. The inset shows a schematic of the experimental brush system.

Table 1. Measured physical properties of polymer brush layers in toluene formed by spin-coating 114k MW PS-P2VP diblocks.

Polymer Thickness (Å)	$\sigma^{*}10^{2}$ (chains Å^{-2})	Measured Brush Extension $2h_{exp}$ (Å)	Overlap Surface Density, $\Sigma^{¥}$	h_{exp}/R_g
54±22	0.015±0.006	620±40	3.0±1.2	**3.9**
182±13	0.051±0.004	720±50	10.0±1.0	**4.5**
209±10	0.058±0.003	800±80	11.4±0.7	**5.0**
228±18	0.063±0.005	840±80	12.5±1.1	**5.3**
289±53	0.080±0.015	1050±100*	15.8±2.9	**6.6**

¥PS/P2VP(57K/57K); N_{PS}=548; R_g=80Å [52]

*An extension of ~550Å was measured for a single brush using neutron reflectivity (Figure 2c)

To more easily evaluate brush behavior as a function of grafting density, the measured force profiles were normalized by the experimentally measured brush extension[9], ($2h_{exp}$), as shown in Figure 4. Although the force profile shape is similar over the Σ range investigated, two distinctly different grafting density regimes are apparent after normalizing the data.

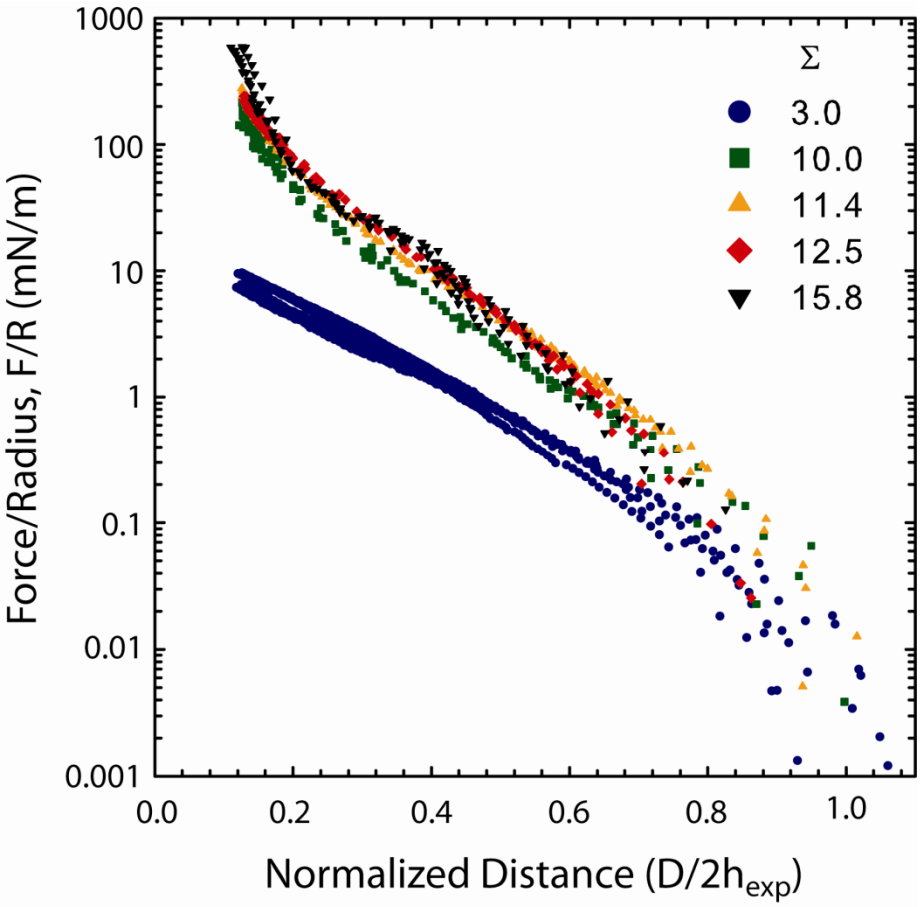

Figure 4. Force profiles of all grafting densities with the distance normalized by the estimated experimental extensions. ($2h_{exp}$).

To qualify these differences, we first compare the measured repulsive force to the self-consistent mean field theory developed by Milner, Witten and Cates (MWC) for two polymer brushes in good solvent conditions[15, 53, 54];

$$F(D)/R = 2\pi h_0 \sigma^{4/3} \omega^{1/3} \nu^{2/3} (1/u + u^2 - u^5/5 - 9/5) \tag{4}$$

where $u=h/h_0$, h_0 is defined as the unperturbed extension of the monodisperse brush calculated from $h_0=(12/\pi^2)^{1/3} N\sigma^{1/3}\omega^{1/3}v^{-1/3}$, ω is the excluded volume parameter, and the effective size parameter ν, which has the dimension of length^{-2}, is found from the statistical segment size, b, using $\nu = 3/b^2$. Based on Alonzo et al.[15] for Σ=3, ω=(3.1Å)^3 and b=8.7Å, while at the highest grafting density Σ=15.8, ω=(3.4Å)^3 and b=7.9Å. To account for polydispersity in a narrow molecular weight distribution system, Milner has suggested using a polydispersity-modified h_0, $h(\Delta)$[54], where

$$h(\Delta) = h_0 \left(1 + \frac{\sqrt{3\left(\frac{M_W}{M_N} - 1\right)}}{2}\right) \tag{5}$$

Substitution of h_0 with $h(\Delta)$ in equation 4 yields a very strightforward means to determine the theoretical force profile while accounting for polydispersity.

The dashed and the solid lines in Figure 3 display the MWC prediction for both a monodisperse brush and polydisperse brush with PDI=1.08. After accounting for the polydispersity, the MWC prediction matches very well to the data at the lowest grafting density, Σ=3. As noted previously[14, 53-55], even a modest chain polydispersity has a signficant effect on the onset of the replusion between opposing polymer brushes as

observed here. In the high grafting density regime, the MWC prediction significantly over-estimates the onset of the repulsion and the magnitude of the experimentally measured force. (All the higher grafting densities showed similar discrepancies. Only Σ=15.8 is reported here for simplicity). A similar overestimaton of MWC theory was observed in earlier work with high density brushes by Ruths et al[37]. In their study, the excluded volume parameter ω was used as an adjustable parameter in the range of $(2.3\text{Å})^3$ to $(3.0\text{Å})^3$ to obtain a more reasonable fit of the MWC prediction to the data. Indeed, a precise value for ω as a function of concentration is not straightforward. Literature values for PS in toluene range from ω = $(2.0$ to $2.3\text{Å})^3$ via light scattering measurements of the second virial coefficient to ω = $(3.2$ Å$)^3$ from osmotic pressure experiments[56, 57]. The excluded volume parameter has great influence on both the predicted force profile and unperturbed brush extension in the MWC theory. Good agreement between our experimental data and MWC theory could also be achieved if the excluded volume parameter was used as a fitting parameter. For our system, this required decreasing ω from $(3.1$ Å$)^3$ at Σ=3 to $(2.5$ Å$)^3$ for Σ=10, but then increasing it slightly to $(2.7$ Å$)^3$ as the grafting density was further increased. Unfortunately, a non-monotonic relationship between the excluded volume parameter and polymer concentration is not consistent with the expected dependence. Regardless, the lower magnitude of the steric force at higher grafting densities and commensurate decrease in the fitted excluded volume parameter suggests that the normally good solvent conditions for PS in toluene are becoming more similar to theta solvent conditions at high PS concentrations. Along these lines, good agreement can be found if the Flory exponent is slightly lowered from

0.595 to 0.565 and calculating a new excluded volume parameter following the development of Alonzo et al.[15].

To further quantify the two observed regimes, we also compared our results to previous models developed by Patel et al.[58] and Watanabe and Tirrell[14] (PTH). The PTH model is based on the well-known scaling model first presented by Alexander and de Gennes (A-dG) [17, 22]. Whereas A-dG assumes the interaction between two opposing, non-interpenetrating brushes is determined by summing the elastic energy and osmotic pressure contributions of the system, the PTH model uses a more realistic form for the osmotic contribution that accounts for good or theta solvent conditions. Thus, universal scaling behavior is expected in the PTH model when the measured force distance profiles are non-dimensionalized using a reduced force **F** and reduced distance **d** defined as:

$$\mathbf{F} = (F/R)/(kT/b^{1/\nu})N\sigma^{(2\nu+1)/2\nu} \tag{6}$$

$$\mathrm{d} = D/2Nb^{1/\nu}\sigma^{(1-\nu)/2\nu} \tag{7}$$

where N is the degree of polymerization; σ is the surface coverage with the unit of chains per area; kT is the thermal energy; b=1.86Å is the monomer size; and the Flory exponent ν=0.595 for good solvent conditions and ν=0.5 for theta solvent conditions [52].

Figure 5 shows the measured force-distance data normalized using the PTH model[58]. Two different regimes are again visible for low and high grafting densities. For comparison, the good and theta solvent predictions of the PTH model are also shown[7,

14]. The good solvent PTH model well represents the low grafting density data (discrepancies at low compressions are due to the PDI of the chains). Very similar behavior was observed by Kilbey et al. and Watanabe and Tirrell[7, 14] on low grafting

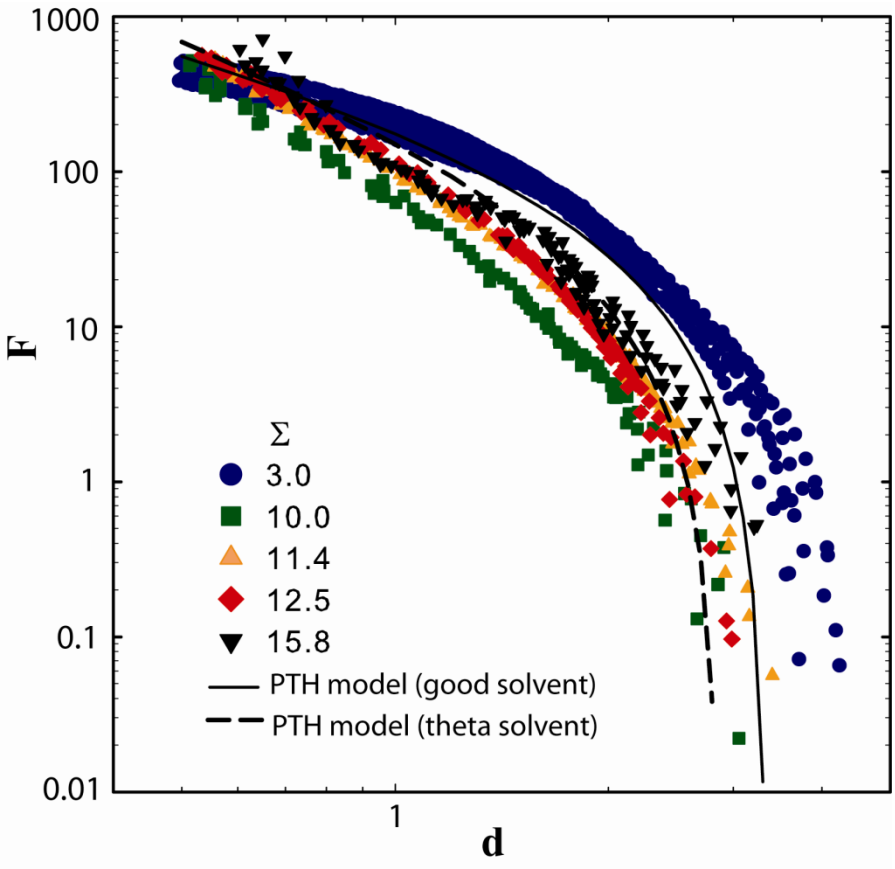

Figure 5. Universal curves for PS-P2VP brushes with different grafting densities in toluene based on the PTH model. The force and distance were scaled using equation 4 and 5, respectively. The PTH model predictions under both good and theta solvent conditions were plotted in the solid line and dashed line, respectively. The parameters suggested in previous literature for the two solvent conditions were applied[7].

density PS-P2VP diblocks of comparable MW. However, the high grafting density regime data deviates from the lower grafting density data yielding a separate curve. Moreover, the high grafting density data is much closer to the theta solvent PTH

prediction. Because the osmotic pressure dominates the elastic force contribution as the brushes are highly compressed, the similarity of the high grafting density regime data and theta solvent conditions suggested by PTH model again indicates that a decrease in solvent quality. This finding is also consistent with a lower excluded volume to properly account for the measured repulsion in the high grafting density regime.

To further demonstrate the different osmotic pressure contributions at high and low grafting densities, one can non-dimensionalize the experimentally measured force profile data (F/R vs. D) with a reduced osmotic energy, $\Delta f_{os,b}$, with respect to the concentration, *c*, where:[14]

$$\Delta f_{os,b} = [(m_0 / N_{AV})^{3\nu/3\nu-1} / (wkT(4\pi b^3/3)^{1/3\nu-1})](1/2\pi)(F/R) \tag{8}$$

$$c = 2\sigma M_{PS} / N_{Av} D \tag{9}$$

Here, m_0 is the PS monomer mass; N_{Av} is the avogadro's number; *w* is defined as the mass of PS chains per unit area which can be computed from the grafting density using $2\sigma M_{PS}/N_{Av}$; and both *b* and *v* have their previous definition. Figure 6 plots the reduced osmotic free energy for the different PS brush grafting densities. Importantly, two different behaviors are again observed for high and low grafting density regimes.

For comparison, the reduced osmotic pressure for a PS homopolymer toluene solution in the semi-dilute regime ($0.05 g/cm^3 < c < 0.15 g/cm^3$) is also shown, [59, 60] where:

$$\pi M_{PS} / ckTN_{Av} = K_\pi (c/c^*)^{1/3\nu-1} \tag{10}$$

and M_{PS} is the molecular weight of the PS block, c^* is the overlap concentration, $c^*=3M/4\pi N_{Av}R_g^3$, and Kπ=2.2 is an empirical constant for PS in toluene[15]. Integrating the osmotic pressure of a PS homopolymer solution given by Eq 10 with respect to distance, yields a simple expression (Eq 11) for the reduced osmotic pressusue ($\Delta f_{os,s}$) of

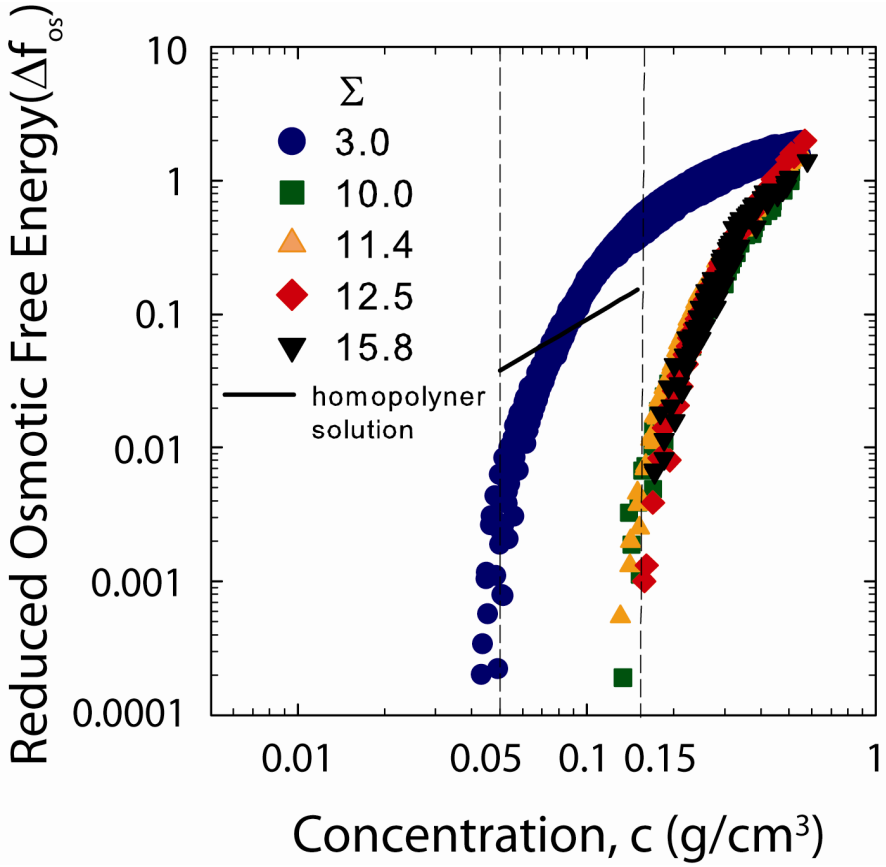

Figure 6. Reduced osmotic free energy for the PS brushes of different grafting densities and the comparison with the PS homopolymer solution. Two dashed lines represent the range of semi-dilute regime suggested by Noda et al[59]. The solid line is the corresponding reduced osmotic free energy for a PS homopolymer solution, Eq. 10.

the PS homopolymer toluene solution as a function of concentration in the semi-dilute range [7, 14] where

$$\Delta f_{os,s} = (3\nu - 1)K_{\pi}c^{1/3\nu-1} \tag{11}$$

As can be seen, the reduced osmotic energy at the lower grafting density, Σ=3, exceeds the predicted homopolymer contribution for concentrations greater than 0.08 g/cm^3. At high compression (high concentration), the slope of the reduced osmotic energy at Σ=3 is consistent with the contribution of PS homopolymer in solution (shown as a solid line). This similarity has been previously observed[7, 14] and indicates consistency with the value of flory exponent (ν=0.595). On the other hand, the average concentration at higher grafting densities , Σ≥10, is close to the limit of the semi-dilute regime (~0.15 g/cm^3) at low compression and exceeds the semi-dilute region with further compression. Compared with the lower grafting density data, the higher slope of the calculated reduced osmotic free energy under compression with the high grafting density data and the fact that all the higher grafting data merge into one curve suggest a smaller value of ν in equation 11. These findings are again consistent with toluene becoming a less good solvent at high PS concentration. A similar decrease in the Flory exponent was found by Zhou and Daivis.[61] Using molecular dynamics they developed a correlation between the concentration of the polymer solution and the flory exponent. In the dilute regime for good solvent conditions, the flory exponent matched well to predictions, ν =0.574. However, ν was found to decrease as the polymer solution concentration increased and the overall solvent quality approached theta solvent conditions, ν = 0.5 for very high concentration, c_p>0.8, where c_p was defined as the fraction of sites occupied by the polymer.

2.5 Conclusion

In this work, spin-coating was used to obtain high grafting density brushes from a single molecular weight diblock. The measured steric force profiles demonstrated two different grafting regime behaviors. At low grafting density, the force profiles were consistent with earlier measurements in the literature and well predicted by the MWC model without adjustable parameters. At high grafting densities, a lower reduced force and higher slope of the reduced osmotic free energy were observed. These findings suggest that the solvent quality of toluene is reduced at high polystyrene concentrations and demonstrate that solvent quality as a function of concentration must be considered to accurately model the data.

2.6 Acknowledgements.

This work was supported by the DOE under Grant No. ER 46340 and benefitted from use of the SPEAR reflectometer and guidance of Dr. Jaroslaw Majewski of the Manuel Lujan Jr. Neutron Scattering Center which is supported by DOE under Contract No. W7405-ENG-36.

2.7 Supporting Information: Neutron Reflectivity Fitting Parameters

Table S1 summarizes the fitting parameters for the SLD profiles shown in the inset of Figure 1a. The neutron reflectivity profiles were fit with the MOTOFIT reflectivity analysis package and nonlinear least-squares regression[46]. For the simple case of a PS-

P2VP film in air, boxes of constant thickness and SLD were used to model the PS and P2VP portion of the thin-film polymer layer. Interfaces were smeared with an error function.

The neutron reflectivity profile of the solvated film was fitted using the MIRROR program developed by Hamilton, which is based on the iterative, dynamical method. [51] The MIRROR program calculates the reflectivity using the optical matrix method from boxes of constant thickness and scattering length density. The corresponding SLD model used to fit the data is based on a power law decay of the brush density Eq 1. In this case, the power law extends from the P2VP layer (Eq. 2) .[13] To account for the polymer tails extending into the solvent, this transitions to a reversed power law (Eq. 3) and then bulk solvent (Eq. 4). The series of equations (Eq 2-4) recapitulate the theoretical predictions for the polymer density profile at a single surface; yet retain sufficient flexibility to allow a variety of profiles to be obtained as dictated by the data. The P2VP anchor block was modeled by two layers: a non-swelled "dry" inner region with an SLD of 1.9 and a slightly solvent-swelled layer with an SLD of 3.07. All the necessary fitting values for establishing the model are shown in Table S2.

$$\phi(x) = \phi_0 \left(1 - \left(\frac{x}{h_0}\right)^n\right) \quad \text{(Eq. 1)}$$

$$SLD(0 \le x \le h_1) = SLD(0) - \left[SLD(0) - SLD(h_1)\right]\left(\frac{x}{h_1}\right)^n \quad \text{(Eq. 2)}$$

$$SLD(h_1 \le x \le h_2) = SLD(h_2) + \left[SLD(h_1) - SLD(h_2)\right]\left(\frac{h_2 - x}{h_2 - h_1}\right)^n \quad \text{(Eq. 3)}$$

$$SLD(h_2 \le x) = SLD_{solvent} \quad \text{(Eq. 4)}$$

where x=0 corresponds to the portion of the brush extending from the P2VP anchor layer, h_1 the endpoint of the first (n_1) power law, and h_2 the endpoint of the second (n_2) reversed power law.

	Quartz		P2VP		PS				
Concentration (g/mL)	SLD, β ($Å^{-2}$ x10 $^{-6}$)	Roughness (Å) Quartz-P2VP	Thickness (Å)	SLD, β ($Å^{-2}$ x10 $^{-6}$)	Roughness (Å) P2VP-PS	Thickness (Å)	SLD, β ($Å^{-2}$ x10 $^{-6}$)	Roughness (Å) PS-Air	χ^2
0.3%	4.2	4	60	1.88	9	63	1.42	4	1.6
0.6%	4.2	6	148	1.89	18	146	1.41	5	2.5
0.8%	4.2	8	163	1.86	24	164	1.40	12	2.9
1.0%	4.2	5	298	1.90	16	235	1.40	89	4.9

Table S2. Single surface fitting parameters of neutron reflectivity measurements in d-toluene for Σ=16

Quartz	Roughness	P2VP		Roughness	Swelled P2VP		Roughness
SLD ($Å^{-2}$ x10 $^{-6}$)	Quartz-P2VP (Å)	Thickness (Å)	SLD, β ($Å^{-2}$ x10 $^{-6}$)	P2VP-Swelled P2VP (Å)	Thickness (Å)	SLD, β ($Å^{-2}$ x10 $^{-6}$)	Swelled P2VP-PS (Å)
4.2	3	19	1.9	7	96	3.07	6

PS							
PS(layer h_1)				PS(layer h_2)			
SLD_0, β ($Å^{-2}$ x10 $^{-6}$)	Thickness (Å)	SLD_1, β ($Å^{-2}$ x10 $^{-6}$)	n_1	Thickness (Å)	SLD_2, β($Å^{-2}$ x10 $^{-6}$)	n_2	χ^2
4.43	191	4.64	2	472	5.5	1.9	2.3

2.8 References and Notes

1. Brochard-Wyart, F., et al., *Adhesion promoters.* J. Phys. Chem., 1994. **98**(38): p. 9405-9410.
2. Klein, J., et al., *Lubrication forces between surfaces bearing polymer brushes.* Macromolecules, 1993. **26**(21): p. 5552-5560.
3. Devaux, C., et al., *Controlled structure and density of "living" polystyrene brushes on flat silica surfaces.* The European Physical Journal E - Soft Matter, 2002. **7**(4): p. 345-352.
4. Milner, S.T., *Polymer Brushes.* Science, 1991. **251**(4996): p. 905-914.
5. Devaux, C., et al., *Low Swelling Capacity of Highly Stretched Polystyrene Brushes.* Macromolecules, 2005. **38**(10): p. 4296-4300.
6. Kilbey, S.M., et al., *Direct Force and Friction Measurements Reflecting Structural Changes in Confined Diblock Copolymer Liquids.* Macromolecules, 1995. **28**(16): p. 5626-5631.
7. Kilbey, S.M., H. Watanabe, and M. Tirrell, *Structure and Scaling of Polymer Brushes near the theta Condition.* Macromolecules, 2001. **34**(15): p. 5249-5259.
8. Tadmor, R., et al., *Sliding Friction with Polymer Brushes.* Physical Review Letters, 2003. **91**(11): p. 115503.
9. Taunton, H.J., et al., *Interactions between surfaces bearing end-adsorbed chains in a good solvent.* Macromolecules, 1990. **23**(2): p. 571-580.

10. Klein, J. and P.F. Luckham, *Variation of effective adsorbed polymer layer thickness with molecular weight in good and poor solvents.* Macromolecules, 1986. **19**(7): p. 2007-2010.

11. Elliott, I.G., et al., *Confined polymer systems: synergies between simulations and neutron scattering experiments.* Soft Matter, 2009. **5**(23): p. 4612-4622.

12. Ell, J.R., et al., *Structural Determination of High Density, ATRP Grown Polystyrene Brushes by Neutron Reflectivity.* Macromolecules, 2009. **42**(24): p. 9523-9527.

13. Mulder, D.J. and T.L. Kuhl, *Polymer brushes in restricted geometries.* Soft Matter, 2010. **6**(21): p. 5401-5407.

14. Watanabe, H. and M. Tirrell, *Measurement of forces in symmetric and asymmetric interactions between diblock copolymer layers adsorbed on mica.* Macromolecules, 1993. **26**(24): p. 6455-6466.

15. Alonzo, J., J.W. Mays, and S.M. Kilbey Ii, *Forces of interaction between surfaces bearing looped polymer brushes in good solvent.* Soft Matter, 2009. **5**(9): p. 1897-1904.

16. Huang, Z., et al., *Impact of Solvent Quality on the Density Profiles of Looped Triblock Copolymer Brushes by Neutron Reflectivity Measurements.* Macromolecules, 2008. **41**(5): p. 1745-1752.

17. Alexander, S., *Adsorption of Chain Molecules with a Polar Head a-Scaling Description.* Journal De Physique, 1977. **38**(8): p. 983-987.

18. de Gennes, P.G., *Conformations of Polymers Attached to an Interface.* Macromolecules, 1980. **13**(5): p. 1069-1075.

19. Milner, S.T., T.A. Witten, and M.E. Cates, *Theory of the grafted polymer brush.* Macromolecules, 1988. **21**(8): p. 2610-2619.

20. Milner, S.T., T.A. Witten, and M.E. Cates, *A Parabolic Density Profile for Grafted Polymers.* EPL (Europhysics Letters), 1988. **5**(5): p. 413-418.

21. Alexander, S., *Polymer adsorption on small spheres: A scaling approach.* Journal de physique., 1977. **38**(8): p. 977-982.

22. de Gennes, P.G., *Polymers at an interface; a simplified view.* Advances in Colloid and Interface Science, 1987. **27**(3-4): p. 189-209.

23. Patel, S., M. Tirrell, and G. Hadziioannou, *A simple model for forces between surfaces bearing grafted polymers applied to data on adsorbed block copolymers.* Colloids and Surfaces, 1988. **31**: p. 157-179.

24. Traskelin, P., T.L. Kuhl, and R. Faller, *Molecular dynamics simulations of polystyrene brushes in dry conditions and in toluene solution.* Physical Chemistry Chemical Physics, 2009. **11**(47): p. 11324-11332.

25. Whitmore, M.D. and J. Noolandi, *Theory of adsorbed block copolymers.* Macromolecules, 1990. **23**(13): p. 3321-3339.

26. Baranowski, R. and M.D. Whitmore, *Numerical self-consistent field study of tethered chains in Theta solvent.* The Journal of Chemical Physics, 1998. **108**(23): p. 9885-9892.

27. Whitmore, M.D. and R. Baranowski, *End-anchored polymers: Compression by different mechanisms and interpenetration of apposing layers.* Macromolecular Theory and Simulations, 2005. **14**(2): p. 75-95.

28. Grest, G.S., *Grafted polymer brushes in polymeric matrices.* The Journal of Chemical Physics, 1996. **105**(13): p. 5532-5541.

29. Pastorino, C., et al., *Static and dynamic properties of the interface between a polymer brush and a melt of identical chains.* J. Chem. Phys., 2006. **124**(6): p. 064902.

30. Elliott, I.G., T.L. Kuhl, and R. Faller, *Molecular Simulation Study of the Structure of High Density Polymer Brushes in Good Solvent.* Macromolecules, 2010. **43**(21): p. 9131-9138.

31. Klein, J., et al., *Reduction of frictional forces between solid surfaces bearing polymer brushes.* Nature, 1994. **370**(6491): p. 634-636.

32. Pelletier, E., et al., *Nanorheology of Adsorbed Diblock Copolymer Layers.* Journal de physique. II, 1997. **7**: p. 271-283.

33. Schorr, P.A., et al., *Shear Forces between Tethered Polymer Chains as a Function of Compression, Sliding Velocity, and Solvent Quality.* Macromolecules, 2003. **36**(2): p. 389-398.

34. Tian, P., et al., *Role of Branching on the Structure of Polymer Brushes Formed from Comb Copolymers.* Macromolecules, 2005. **38**(6): p. 2524-2529.

35. Kent, M.S., et al., *Tethered chains in good solvent conditions: An experimental study involving Langmuir diblock copolymer monolayers.* The Journal of Chemical Physics, 1995. **103**(6): p. 2320-2342.

36. Kent, M.S., *A quantitative study of tethered chains in various solution conditions using Langmuir diblock copolymer monolayers.* Macromolecular Rapid Communications, 2000. **21**(6): p. 243-270.

37. Ruths, M., et al., *Repulsive Forces and Relaxation on Compression of Entangled, Polydisperse Polystyrene Brushes.* Macromolecules, 2000. **33**(10): p. 3860-3870.

38. Samadi, A., et al., *Low-Temperature Growth of Thick Polystyrene Brushes via ATRP.* Macromolecular Rapid Communications, 2005. **26**(23): p. 1829-1834.

39. Baranowski, R. and M.D. Whitmore, *Theory of the structure of adsorbed block copolymers: Detailed comparison with experiment.* The Journal of Chemical Physics, 1995. **103**(6): p. 2343-2353.

40. Koneripalli, N., et al., *Confined Block Copolymer Thin Films.* Macromolecules, 1995. **28**(8): p. 2897-2904.

41. Levicky, R., et al., *Concentration Profiles in Densely Tethered Polymer Brushes.* Macromolecules, 1998. **31**(11): p. 3731-3734.

42. Hamilton, W.A., et al., *Determining the density profile of confined polymer brushes with neutron reflectivity.* Journal of Polymer Science Part B: Polymer Physics, 2004. **42**(17): p. 3290-3301.

43. Dubey, M., et al., *SPEAR — ToF neutron reflectometer at the Los Alamos Neutron Science Center.* The European Physical Journal Plus, 2011. **126**(11): p. 1-11.

44. Smith, G.S., et al., Los Alamos Neutron Scattering Center News Lett, 1993. **15**: p. 5.

45. Russell, T.P., *X-ray and neutron reflectivity for the investigation of polymers.* Materials Science Reports, 1990. **5**(4): p. 171-271.

46. Nelson, A., *Co-refinement of multiple-contrast neutron/X-ray reflectivity data using MOTOFIT*, in *Journal of Applied Crystallography*2006, Blackwell Publishing Limited. p. 273-276.

47. Israelachvili, J.N., *Thin film studies using multiple-beam interferometry.* Journal of Colloid and Interface Science, 1973. **44**(2): p. 259-272.

48. Israelachvili, J.N. and G.E. Adams, *Direct measurement of long range forces between two mica surfaces in aqueous KNO3 solutions.* Nature, 1976. **262**(5571): p. 774-776.

49. Israelachvili, J.N. and G.E. Adams, *Measurement of forces between two mica surfaces in aqueous electrolyte solutions in the range 0–100 nm.* J. Chem. Soc., Faraday Trans., 1978. **1**(74): p. 975 - 1001.

50. Derjaguin, B.V., Kolloid Zeits, 1934. **69**: p. 155-164.

51. The fitting program used for this data is an eponymous integral data collection and profile modelling analysis package for the MIRROR neutron reflectometer developed by W.A. Hamilton and J.B. Hayter (1992-2003). The statistical and error estimation concepts used therein are described in P.R. Bevington Data Reduction and Error Analysis for the Physical Sciences (McGraw-Hill, New York, 1969) Chapter 11 and in W.H. Press, S.A. Teukolsky, W.T. Vetterling and B.P. Flannery, Numerical Recipes in Pascal (Cambridge University Press, Cambridge, 1989), Chapter 15. The minimization routine employed by the MIRROR program is the ‘‘downhill simplex’’ method of J.A. Nelder and R. Mead, Computer Journal 7, 308 (1965), in an implementation described in Chapter 104 of Numerical Recipes.

.

52. Higo, Y., N. Ueno, and I. Noda, *osmotic pressure of semidilute solutions of branched polymers.* polymer journal, 1983. **15**(5): p. 367-375.

53. Milner, S.T., T.A. Witten, and M.E. Cates, *Effects of polydispersity in the end-grafted polymer brush.* Macromolecules, 1989. **22**(2): p. 853-861.

54. Milner, S.T., *Compressing polymer brushes—a quantitative comparison of theory and experiment.* Europhysics Letters, 1988. **7**: p. 695-699.

55. Alonzo, J., et al., *Kinetics of assembly of "looped" polymer brushes at the solid-fluid interface.* Abstracts of Papers of the American Chemical Society, 2005. **230**: p. U3527-U3527.

56. Brandrup, J., Immergut, E. H., Polymer Handbook, 3rd ed., 1989.

57. Kuwahara, N., T. Okazawa, and M. Kaneko, *Excluded-Volume Effect of Polystyrene Solutions.* J. Chem. Phys., 1967. **47**(9): p. 3357-3360.

58. Patel, S., M. Tirrell, and G. Hadziioannou, *A simple model for forces between surfaces bearing grafted polymers applied to data on adsorbed block copolymers.* Colloids and Surfaces, 1988. **31**(0): p. 157-179.

59. Noda, I., et al., *Semidilute region for linear polymers in good solvents.* Macromolecules, 1984. **17**(5): p. 1055-1059.

60. Noda, I., et al., Macromolecules, 1981. **14**: p. 668-676.

61. Zhou, Z.W. and P.J. Daivis, *Molecular dynamics study of polymer conformation as a function of concentration and solvent quality.* Journal of Chemical Physics, 2009. **130**(22): p. 224904-1~224904-10.

Chapter 3: Normal and Shear Interactions between High Grafting Density Polymer Brushes Grown by Atom Transfer Radical Polymerization

Submitted to Soft Matter, August 21st, 2012, under the same title, with authors (in order): Wei-Po Liao, Ian Elliott, and Tonya Kuhl.

3.1 Abstract

The normal and shear interactions in toluene of polystyrene polymer brushes with ultra-high surface coverage ranging from 15 to 70 mg/m^2 formed by atom transfer radical polymerization were measured with a surface force apparatus. Significant hysteresis was observed between compression and separation cycles over the experiment time scale for all surface coverages. The magnitude of the hysteresis increased with increasing film thickness. The experimental relaxation time of the thickest brush layer was at least four orders of magnitude longer than that predicted by the Rouse model. Remarkably, the shear performance of the thickest brushes still demonstrated very good lubricity under compressions down to 35% solvent content. These findings are consistent with a reduction in solvent quality with compression leading to a shrinkage or collapse of the brush under high compression, while still maintaining a region of well solvated chains in the overlap region between the brushes. Thus, hysteresis in compression is primarily due to intra-brush entanglements and collapse of the brush layer rather than inter-brush entanglements and brush-brush interpenetration.

3.2 Introduction

Polymer brushes are frequently used to modify interfacial properties where they can act as steric stabilizers, adhesion modifiers, or enhance lubricity.[1-3] A polymer brush is formed when one end of the chain is confined to the interface or surface and the spacing between these anchor points is smaller than the polymer chain's radius of gyration, R_g. As the spacing between neighboring chains decreases, the chains are forced to stretch away normal to the grafting surface to decrease crowding. These structural changes due to osmotic crowding result in very different behaviors from free polymer chains in solution.[4, 5] In typical experiments, the polymer brush layer is formed by a "grafting to" approach in which chains are selectively anchored to the surface through physical adsorption methods that rely on diblock polymer chains and preferential solvation or by functionalizing the chain end leading to strong electrostatic binding or chemical bond formation to the surface. In both cases, the grafting density of the brush is limited by steric hindrance between the surface grafted chains. [6]

Because the brush structure and its physical properties depend intimately on the chain molecular weight, surface coverage, and solvent quality,[7-9] polymer brushes can be used to tailor interfacial properties[1-3]. Motivated by the wide application potential of polymer brush systems, a large number of theoretical,[5, 10-14] experimental[15-19] and simulation[20-25] studies have been carried out in order to characterize and ultimately predict the properties of polymer brushes. In particular, the tribological behavior of polymer-bearing surfaces has drawn significant attention as ultra-low friction coatings.[26-31] For example, Klein et al[26] found that the friction coefficient between

mica surfaces grafted with end-functionalized Polystyrene (PS) brushes in good solvent conditions was two orders of magnitude lower than that of bare mica in toluene. Similarly, Raviv et al.[28] found similar low friction behavior with physically adsorbed poly(ethylene oxide) (PEO) bearing surfaces in good solvent condition under moderate compressions. For high shear rates and high compression, some loss of the polymer brush layer was observed and a transition of the shear interface from polymer/polymer to polymer/substrate was suggested. A detailed comparison of normal and shear behavior in good and theta solvent conditions was carried out by Schorr et al[31] using amphiphilic polystyrene-poly(vinylpyridine) (PS/P2VP) diblocks. The best lubricant performance was found for good solvent conditions and shear-thinning behavior was observed with increasing sliding velocity. Using the same system, Forster et al.[32] found similar behavior where the onset of detectable shear force was found to shift to higher compression ratios as the solvent quality increased. Thus, the compression and interpenetration of opposing brush layers plays an important role in their frictional properties and the extent of interpenetration has been shown to increase with compression ratio and grafting density.[29, 33, 34] At a molecular level, recent molecular dynamic simulations have directly linked better lubrication behavior in good solvent conditions to fewer inter-brush contacts.[35] However, these previous studies were on dilute to semi-dilute brushes and the properties of ultra-high grafting density brushes have not yet been systematically studied.

Intrinsically, steric overlap between neighboring chains limits “grafting-to” polymer brushes to the dilute or semi-dilute grafting density regime. This can constrain the practical application needs of a stable and durable surface, particularly under high

load. In contrast, the "grafting from" method where the polymer chain grows monomer by monomer from a surface using living polymerizations[36] can yield much higher grafting densities. However, only a handful of experiments have studied brush properties in this regime. Ruth et al[37] performed the first comprehensive measurements of the interaction force between "grafting-from" brushes by replacing the chemically inert mica surfaces typically used in the surface force apparatus (SFA) with thin silica films that could be functionalized with a covalently grafted ATRP initiator layer. High molecular weight polystyrene brushes were grown directly on the surfaces, however the high polydispersity of the chains made quantitative comparison to polymer theory challenging.[38] Subsequently, Yamamoto et al.[39, 40] investigated Poly(methyl methacrylate) (PMMA) brushes by AFM. Discrepancies between the experimentally measured force-distance profile and scaling predictions[41] were attributed to the fact that the polymer concentration under this highly grafted condition significantly exceeded the semi-dilute concentration range assumptions used in the scaling theory. The tribology properties of "grafted from" brushes have primarily been investigated macroscopically[42-44] using conventional ball-on-disk type tribometers. Sakata et al.[43] measured PMMA brushes in different solvent conditions including the dry state. As in the microscopic SFA measurements, the lowest dynamic friction coefficient was found in good solvent conditions. In contrast, Kobayashi et al[42] found that the high density brushes of biocompatible polymer 2-methacryloyloxyethyl phosphorylcholine (MPC) had the best lubricant performance when in a high-humidity environment rather than when fully solvated in bulk water. They hypothesized that the dense brushes interpenetrated more in bulk water leading to higher friction compared to brushes in high

humidity. Recently, Dunlop et al.[45] demonstrated a means to functionalize mica surfaces with a strongly absorbed poly-initiator film in order to obtain high grafting densities of a surface-grown polyelectrolyte brushes of poly [2-(Methacryoyloxy)ethyl][29, 46] trimethylammonium chloride (poly(METAC)). A small hysteresis was observed between the polyelectrolyte brushes during compression-decompression which was attributed to attractive bridging interactions. Frictional properties were similar to earlier studies on polyelectrolyte brushes. This approach opens a straightforward means to carryout high resolution SFA experiments on high grafting density polymer layers.

In this work, an SFA was used to measure the normal and shear forces of high density "grafted from" polystyrene chains in toluene, a good solvent for polystyrene. The brushes were grown from silica films electron-beam deposited on mica enabling higher film thicknesses and grafting densities to be studied, while still preserving the high force and distance resolution of the SFA technique. In contrast to previous work on "grafted to" brushes at lower grafting densities that have primarily shown reversible compression forces, significant hysteresis was observed in the high density, "grafted from" system. The hysteresis, however, did not correlate with an increased friction between the brushes during shear force measurements at modest solvation. The work demonstrates that ultra-high density polymer brushes provide a very robust, low friction coating even under conditions where solvent quality is significantly reduced.

3.3 Experimental Section

3.3.1 *Surface Functionalization of Mica*

To provide an appropriate substrate for ATRP synthesis of the grafted from polymer brush chains, a thin-coating of silica was electron beam (E-beam, AUTO-TECH II, CHA industries) deposited on freshly cleaved sheets of mica. The procedure used followed the methodology described by Vigil et al.[47] In the present work, the silica layer was 1000Å silica layer. The thickness and the refractive index of the silica layer were further confirmed by ellipsometry (EL2, Rudolph) yielding values of thickness and the refractive index of 1048±12Å and 1.48±0.01, respectively. The peak-to-valley roughness of the deposited silica was 5Å as determined by AFM and is consistent with the number previously reported by Vigil et al. The silica film was found to swell ~4% in bulk water.

The thickness and refractive index of the silica film was also characterized in the SFA using multiple beam interferometry prior to ATRP polymer film growth. Freshly cleaved mica with the desired thickness and size was first cut into one or two larger pieces (few cm^2) and one smaller piece (few mm^2). The smaller piece was not coated with silica and used as a reference system to determine the mica substrate thickness. Silica was then deposited on the larger mica piece(s). After silica deposition, the mica pieces were flipped and placed on another mica backing sheet. A ~550Å of silver layer was deposited on the mica side of both the small mica pieces and the silica deposited mica pieces. The coated mica surfaces were then glued, silver side down, onto cylindrically curved glass disks using an optical adhesive (NOA 61, Norland Product Inc.) and cured by exposure to UV light for 5 minutes. Details of the thickness and refractive index determination by

multiple beam interferometry are provided later under the heading *Thickness Determination*.

3.3.2 *Atom Transfer Radical Polymerization*

Materials. Styrene was purchased from Fisher Scientific, Karstedt catalyst was purchased from Gelest, and all other chemicals were from Sigma-Aldrich. Styrene was stirred with CaH_2 overnight to remove any water and vacuum distilled to remove the inhibitor. The distilled styrene was stored at 4°C under nitrogen. CuBr was stirred over glacial acetic acid overnight, filtered, and washed with large quantities of ethanol.

3.3.3 *10-undecenyl 2-bromoisobutyrate Synthesis*

10-undecenyl 2-bromoisobutyrate, a precursor required for the initiator synthesis, was synthesized following the work of Matyjaszewski.[48] A stir bar, 5.9 mL 10-undecen-1-ol, 5.3 mL triethylamine, and 50 mL dichloromethane were added to a 100 mL round bottom flask in an ice bath. 3.7 mL 2-bromoisobutyryl bromide were added to the flask dropwise over a period of 5 minutes. The flask was removed from the ice bath and stirred at room temperature for 15 hours. The solution was washed with 65 mL of 0.5 molar HCL, and then washed with 65 mL DI water 3 times. Solvent was removed by rotovap. The solution was run through a column of silica gel with 100 mL of a 25:1 hexane:ethyl acetate solvent solution. The solution was again rotovaped to remove hexane. This procedure yielded approximately 7.5 g of a clear liquid.

3.3.4 *Initiator Synthesis*

The surface active initiator 11-(2-Bromo-2-methyl)propionyloxy)undecyl trichlorosilane was synthesized following previous work.[49] 4.6 mL of 10-undecenyl 2-bromoisobutyrate and a stir bar were added to a 50 mL schlenk flask. The flask was sealed and purged with nitrogen. Three freeze-pump-thaw cycles followed to ensure no oxygen was in the flask or liquid. 82 μL of Karstedt catalyst (2.1-2.4% Pt in xylene) were added and the flask was transferred to an ice bath. 4.75 mL trichlorosilane was added dropwise to the solution. The flask was allowed to slowly warm to room temperature and stirred for five hours under nitrogen. The product was transferred to a round bottom flask and vacuum distilled at 30 mtorr. The distillation yielded 2.72 grams of initiator.

3.3.5 *Initiator deposition*

The silica surfaces glued on the SFA discs were cleaned prior to initiator deposition by stirring in acetone for 10 minutes, followed by rinsing with isopropyl alcohol, Millipore filtered water, pure ethanol, and then dried with nitrogen. The surfaces were then exposed to UV/ozone for 20 minutes to hydroxilate the surfaces. Afterwards, the substrates were placed in a gently stirred solution of 34 μL 11-(2-Bromo-2-methyl)propionyloxy)undecyl trichlorosilane in 50 mL toluene for one hour. Upon removal of the substrates, partial dewetting of the toluene solution at the edge of the surfaces was evident of the formation of a self-assembled layer of initiator. The surfaces were then immediately rinsed in clean toluene (5-10 minute immersion with gentle stirring), removed and dried with nitrogen. Finally, the dry initiator coated surfaces were

annealed at 75ºC to promote cross-polymerization and robust attachment of the initiator layer.

3.3.6 *Polymerization*

End-grafted polystyrene chains were synthesized from the initiator coated surfaces using established procedures.[49, 50] A custom reaction flask was used which could be taken apart to add or remove the surfaces.[49] After placing the surfaces in the reaction flask, 124 mg CuBr, 10 mg $CuBr_2$, and a stir bar were added. The flask was sealed and evacuated and backfilled with nitrogen three times. In a separate schlenk flask 10 mL styrene, 5 mL toluene, and 189 μL N,N,N',N',N"-Pentamethyldiethylenetriamine (PMDETA) were added and oxygen was removed by performing three Freeze-Pump-Thaw cycles. Afterwards, 13 μL ethyl 2-bromoisobutyrate were added to the flask, and the solution was immediately transferred to the custom reaction flask at 90°C using a syringe. The reaction was allowed to proceed for a designated time, generally three to eight hours. To quench the reaction at the designated time, the heat was turned off, the solution was exposed to air, and THF was added. Finally, the surfaces were stirred in hot toluene for 20 minutes to remove unreacted monomer and stirred in IPA for 20 minutes to remove copper salts.

3.3.7 *Surface Force Apparatus*

The surface force apparatus (SFA) technique has been widely used for measuring the interactions between two opposing surfaces as a function of separation and details of the instrument and measurements have been explicitly described elsewhere.[51-55] Briefly, the interaction forces are obtained by determining the deflection of a force measuring

spring supporting the lower surface while the distance between two surfaces are measured by monitoring the fringes of equal chromatic order (FECO) using a spectrometer. The polymer coated discs are placed in cross cylinder geometry and the measured radius of surface curvature for each contact position was used to normalize the measured force to enable quantitative comparison between different contact positions and experiments. The Derjaguin approximation[56] gives the relationship between the interaction energy per unit area, E, for two flat plates from the measured force-distance, $F(D)$, relationship between two crossed cylinders

$$E(D) = \frac{F(D)}{2\pi R} \tag{1}$$

The Derjaguin approximation is valid at small distances where $D << R$. The radius of curvature was measured for two cross sections, at 90º and the geometrical mean was used in calculations. For these experiments the measured radius of curvature was 1.0 ± 0.15 cm.

In the present work, normal and shear force profiles between the ATRP grown brushes were measured by a Mark II SFA with a shear device (by SurForce). The shear device includes both a receiver where the top surface was mounted and a bimorph slider device where the lower surface was mounted. As in previous designs[57, 58], application of a triangular signal to the bimorph slider enables linear lateral movement of the lower surface relative to the upper surface, here up to 1mm.[58] The top receiver assembly has semi-conductor strain gauges to work as a force sensor.

3.3.8 *Thickness Determination*

The thickness in air and the refractive index of the layers was determined by the FECO wavelength positions using a multi-matrix method (MMM)[59] and additional details are provided elsewhere.[60] Briefly, a model of the optical cavity is used to generate the FECO wavelength pattern by MMM with input parameters such as thickness and refractive index of each layer. A fitting algorithm determines the set of parameters that minimizes the difference between the experimental measurement and the model. Figure 1 provides an example of the contact fringes obtained from the corresponding geometries of the system where subsequent layers are added to demonstrate how the thickness and refractive index of the various layers (silver, mica, silica, polymer) were determined. First, the bare mica-mica contact (a) was always measured as a control in order to determine the thickness and the refractive index of the silver and mica sheets before adding subsequent layers, e.g. silica and polymer. Next, the contact of silica-silica (b) was measured for identical mica sheets and the thickness and refractive index of the deposited silica film was determined. The accuracy of the fitting program and approach was confirmed by comparing the thickness obtained from ellipsometry to that of multiple experiments with different mica and silica thicknesses. Throughout any given experiment, differences between the control measurements before and after adding additional optical layers were less than 3% in thickness and 1% in refractive index. After establishing the thicknesses and refractive indexes of the silver, mica, and silica layers, the thickness of the ATRP-grown polystyrene was determined be simply fitting the FECO wavelengths of the entire system (c). At least four different positions on the surfaces of different sets of samples were measured to confirm the uniformity of the film.

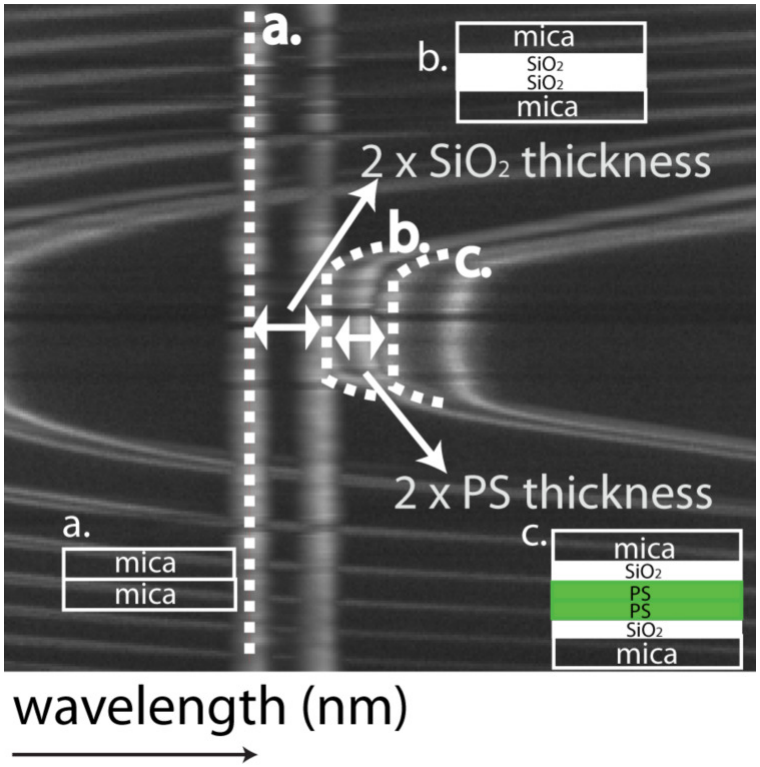

Figure 1. An example image of how the fringes of equal chromatic order (FECO) wavelengths shift as the number of layers between the surfaces is increased. The optical cavity between the silver layers is modeled and the data fitted to extract the thicknesses and refractive index of the different layers (silver, mica, silica, and polymer) sequentially. The image itself is an overlay of the contact FECO wavelengths for the three measured geometries used; (a) contact of mica-mica surfaces, (b) contact of silica-silica surfaces, (c) contact of PS-PS surfaces. The dashed lines are guides to distinguish different contact geometries.

3.3.9 *Normal and Shear Force Measurements of Polymer Layers*

In the normal force setting, after the measurements of the dry PS film thickness, the surfaces were separated a couple of millimeters and the SFA was filled with toluene. The surfaces were brought closer together (≤0.5mm) and the film was left solvating for 24 hours before measuring the force profile. The distance "D" utilized in the force-distance profiles provided in the following sections was defined as the spacing between the

opposing silica surfaces which corresponds directly to the thickness or extension of the two PS brushes. Multiple compression-decompression cycles for different positions on the surfaces were measured. At least 10 seconds was elapsed after each displacement before taking a reading of the surface separation and 30 minutes was elapsed between different approach/separation cycles to allow for chain relaxation. As is commonly done, the shear force measurements used a droplet of toluene as the shear attachment cannot be fully immersed in solvent.[16] A small vial of toluene was placed inside the SFA chamber during shear measurements to maintain the vapor pressure and prevent evaporation of the toluene droplet between the surfaces. The lateral, parallel movements of the lower surface mounted in the bimorph device were achieved by applying a triangular signal with a function generator (3325B, Hewlett Packard) while a signal conditioning amplifier (2300, Vishey) was used to magnify the signal obtained from the receiver where the upper surface was mounted. The magnified response voltage was collected by a XYt chart recorder (BD41, Kipp&Zonen) and converted to the force (N) between the surfaces. An example of the XYt output is shown in Figure 2. The applied triangular signal and the detected voltage were monitored simultaneously. The sliding distance and the velocity of the lateral motion from the lower surfaces were controlled by the applied voltage and the frequency of the function generator, respectively. In the present work, the maximum sliding distance was fixed at 1.25μm while the velocity was 100nm/s.

For several measurements, the normal force profile was measured in both the normal and shear force setting to confirm reproducibility, and that the brush layers remained fully

solvated in toluene throughout the droplet experiment. The normal force profile and the film thickness were also checked before and after the shear measurements to confirm the

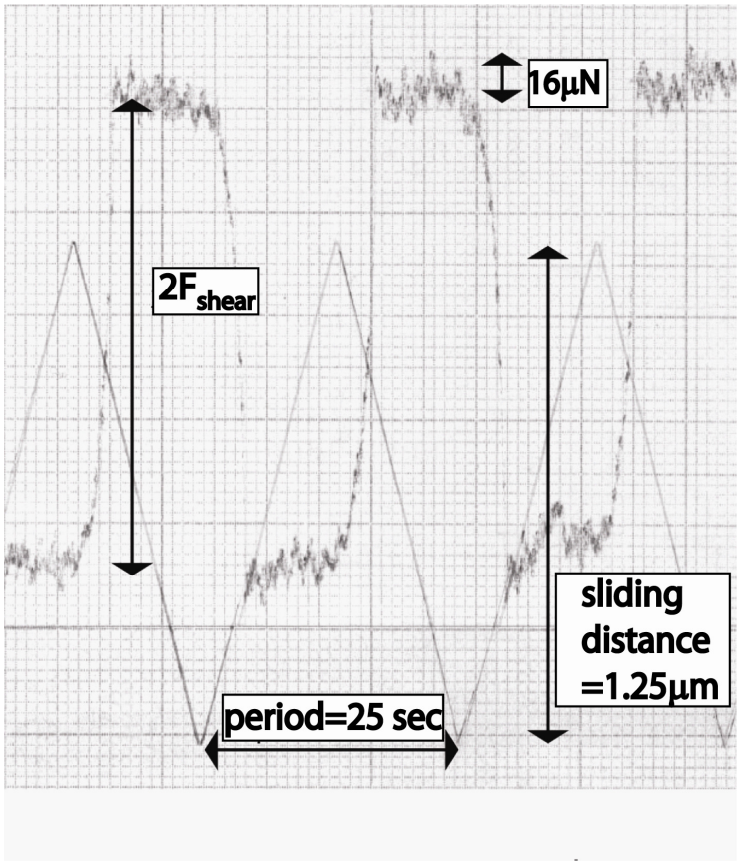

Figure 2. Example of a XYt plot used for shear force analysis of ATRP grown PS brushes (D=1767±33Å). The maximum sliding distance was 1.25 μm obtained from the peak-to-peak value of the triangular wave. The shear force between the opposing PS brushes is denoted as F_{shear} and is determined from the plateau height difference.

stability of the ATRP grown PS brushes. No substantive change in thickness was detected. Both the shear and normal force measurement were performed in a temperature controlled environment at 25±0.2°C.

3.4 Results and Discussions

3.4.1 *Brush Properties*

In this work, the physical properties of ultra-high density PS brushes formed by the "grafting from" method were studied using an SFA. The dimensionless overlap surface density, $\Sigma=\sigma\pi R_g^2$, is typically used to describe and compare different brushes, where σ is the experimental chain grafting density (chains/Å^2), and R_g is the radius of gyration of a free polymer chain in solution[20]. A clear challenge in using "grafting from" brushes is defining the MW and grafting density of the formed polymer brush layer. Fortunately, it is straightforward to measure the dry film thickness and uniformity of the grown film using SFA measurements. Table 1 reports the average measured polymer thickness for three different ATRP grown PS films. The error was established by measuring the film thickness at a minimum of 4 different contact positions between the layers. Given the bulk density of PS, $\rho=1.05 g/cm^3$, the mass per unit area of the grown PS film can be easily calculated from the measured dry thickness. To provide information on the MW of the brush layer, free initiator was present in the reaction solution during our polymerizations. It has been previously reported that chains grown free in solution provide a good indication of the MW of chains grown simultaneously from initiator

layers from the surface.[49, 61-63] The MW and PDI of the free chains in the polymerization supernatant were determined by GPC.

These values versus the measured dry film thickness are reported in Table 1 and plotted in the inset of Figure 3. Typically, a linear increase in dry film thickness with MW is expected and has been reported in earlier studies. In this work, the two lower MW polymerizations follow a linear increase in film thickness. However, the thickest film, which also had the highest PDI, clearly deviates significantly from this trend. This deviation at high polymerizations is attributed to termination events in the surface film. Even with this caveat, the supernatant measurements of MW and PDI do provide an estimate of the surface grown polymer film properties and three clearly different conditions were achieved (Table 1). The calculated value of Σ~191 for the thickest film is likely a significant overestimation. Based on the measured film thickness, a more modest MW of ~100k yields an Σ~162.

3.4.2 *Force Profile Measurements*

Next, the interaction force profiles as a function of distance for three different ATRP grown PS films in toluene are described. As will be discussed in the next section, significant hysteresis was observed in the normal force measurements. The data reported in Figure 3 were measured after allowing the systems to relax for at least 24 hours before compressing. The extension of the brush in toluene, as depicted by the arrows in Figure 3, was defined as the onset of the repulsive force under these equilibrated conditions (Table 1). The onset distance increases with the thickness of the dry PS film, consistent with the

Table 1. Characterizations of the ATRP grown Polystyrene

	SFA Measured			GPC Measured		Estimated		
Sample	PS Dry Thickness (Å)	Measured Brush Extension h_{exp}, (Å)	mg/m^2	MW (Kg/mole)	PDI	$\sigma x10^2$ (chains Å^{-2})	Overlap Surface Density Σ^*	**Fully Stretched Length L¥, (Å)**
A	142±13	630±50	15±1.3	23.5	1.088	0.38	26	**588**
B	502±36	1950±100	52±3.1	60.5	1.211	0.52	111	**1513**
C	665±41	2370±125	70±4.5	100.0$^{\Delta}$	1.285	0.18	162	**2500**
D§	73±13	525±50	7.6±1.0	57.0	1.080	0.08	15.8	**1425**

*Rg=1.86 x N$^{0.595}$, where N=degree of polymerization[64]

§Physically adsorbed brush formed from a 50:50 PS-P2VP diblock copolymer

¥L=aN where a is the repeating PS monomer size of 2.6Å.[9]

$^{\Delta}$ Estimated based on the inset of Figure 1 measured by GPC.

expected increase in the grafted brush MW with increasing film thickness. With further compression, the repulsive force increased monotonically with decreasing separation. One fact that needs to be noted here is that unlike the grafting-to brushes, the extensions of the ATRP grown PS were very close or even exceeded the fully-stretched length based on the GPC measurements. Although the PDI of the chains can account for this discrepancy, the GPC results from the supernatant chains should only be considered a

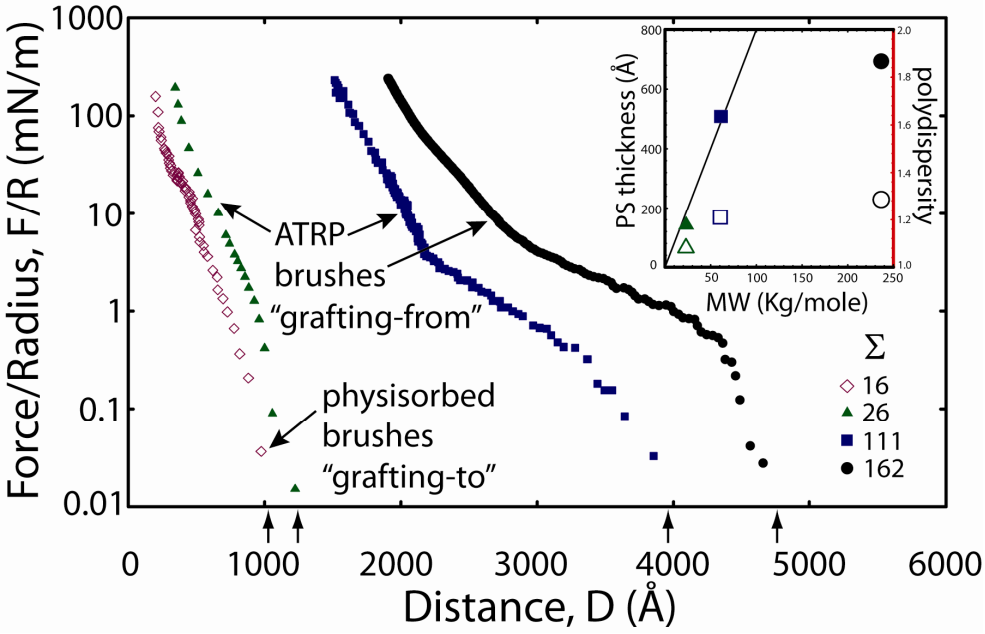

Figure 3. Measured force profiles of ATRP grown PS brushes for three different grafting densities (solid symbols). Force profile data for a well-defined brush formed from a 50:50 PS-P2VP diblock copolymer with Σ=16 (diamonds) is also shown for comparison. The inset shows the relationships among dry PS thickness (closed symbols), MW and the polydispersity (opened symbols) determined by GPC.

rough indication of the MW and PDI of the surface grafted chains. The primary characterization of the surface films is obtained by direct measurement of the film thickness and solvated brush extension by SFA.

For comparison, the force to compress a physically adsorbed brush formed from a 50:50 polystyrene-b-poly-(2-vinylpyridine) (PS-P2VP) diblock copolymer with Σ=16 is also shown. The physical properties of this well-defined "grafted to" brush are also provided in Table 1. As can be seen, the force profile for this PS-P2VP brush (PS MW = 57k) is very similar to that of the Σ~26 ATRP PS brush ($MW_{estimate}$=23.5k). Moreover, both the ~PDI and dry film thickness are very similar for both of these cases although their MWs may differ by almost a factor of 3. In contrast, the high MW ATRP brushes (Σ~111, 162) have a much softer long-range repulsion due to their higher PDI and MW. This soft repulsion further suggests that the GPC measurements should be considered as a lower bound estimate for the grafted brush PDI. Although the MW of the PS diblock matches the Σ~111 ATRP PS brush ($MW_{estimate}$=60.5k), the brush extension is much longer with the ATRP brush due to the presumably large increase in grafting density. To the best of our knowledge, these are the highest grafting density brushes for which interaction force profiles have been measured.

The measured repulsive force was also compared to the self-consistent mean field theory developed by Milner, Witten and Cates (MWC) for two polymer brushes in good solvent conditions[18, 38, 65];

$$F(D)/R=2\pi h_0\sigma^{4/3}\nu^{2/3}\omega^{1/3}(1/u+u^2-u^5/5-9/5)$$

where $u=h/h_0$, h_0 is defined as the unperturbed extension of the monodisperse brush calculated from $h_0=(12/\pi^2)^{1/3}N\sigma^{1/3}\omega^{1/3}\nu^{-1/3}$, ω is the excluded volume parameter, and the effective size parameter ν, which has the dimension of length^{-2}, is found from the statistical segment size, b , using $\nu=3/b^2$. The values of ω and b used were (3.2Å)^3 and

7.6Å, respectively, based on the work with a similar ATRP system carried out by Ell et al.[49] As shown in Figure 4 for Σ~26 the MWC prediction matches reasonably well to the measured force after repeated compression and separation cycles. As originally demonstrated by Milner and subsequently others,[37, 66, 67] a small increase in the chain PDI leads to a significant increase in the onset of the measured repulsion between opposing polymer brushes as observed here. It is, however, somewhat surprising that the MWC theory provides a reasonable estimate given that the theory assumes dilute/semi-

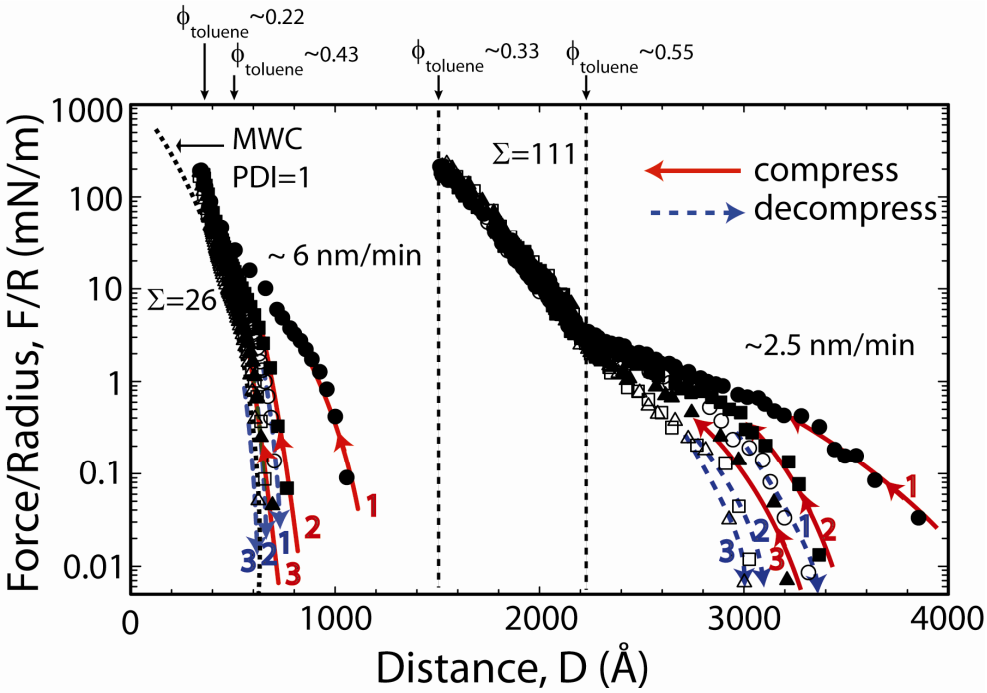

Figure 4. Compression/decompression cycles for forces profiles of two opposing ATRP grown PS brushes in toluene with overlap surface density Σ=26 and 111. Solid symbols and empty symbols with corresponding shapes represent a single compression and decompression cycle, respectively. The solid and dashed lines with arrowheads are the guides to the eye. At least 30 minutes between different cycles and 8-12 seconds between each surface displacement were allowed for brush relaxation. The average approach rates for each system are provided. The long-dashed line shows the predictions of mono-disperse MWC theory for Σ=26.

dilute polymer concentration and simple pairwise interactions. The strong stretching limit is likely more reasonable for these high grafting density brushes than more typical, lower density "grafting-to" brushes.[66] Based on our estimated grafting density of Σ~26, the average concentration of the polymer was already significantly above the limit of the semi-dilute concentration range.[68] Not surprisingly, at the higher grafting densities, Σ~111 and 162, the agreement was very poor. However, the MW and polydispersity of the grafted brushes may not be well represented by the measured values for free chains in solution during the polymerization. For thicker films, it is more difficult to maintain a constant growth rate and there is a greater chance for chain transfer termination events between neighboring chains.[69]

A more interesting feature of the grafted brushes is the significant hysteresis observed in the force profiles, where the measured interaction force upon separation was much less than that on surface approach. Such behavior has only rarely been reported between end-grafted polymer brushes in good solvent conditions. Indeed, the only examples we are aware of also studied polydisperse, "grafting-from" polymer brushes[37, 45, 70] and "grafting-to" system with high MW and polydispersity.[28, 70] More commonly, hysteresis is observed under poor solvent conditions where the polymer layers are somewhat adhesive; when there is incomplete brush coverage on the surfaces resulting in bridging interactions; or, the polymer film is absorbed and undergoes long-lived structural rearrangements during the measurements. Examples of compression decompression cycles of our ATRP brushes are shown in Figure 4 for Σ~26 and Σ~111. The solid and empty symbols represent the compression and decompression processes, respectively, while the solid and dashed lines with arrow heads are provided as a guide to

distinguish different approach and separation cycles. The initial compression was carried out on equilibrated brushes that had been allowed to relax for at least 24 hours before compressing. After each surface displacement during the force measurement, the brushes were allowed to relax for 8-12 seconds before measuring the surface separation. The average approach rate is reported in Figure 2. Similar behavior is observed for the three ATRP brush systems where the brush extension becomes less for subsequent compression decompression cycles. The magnitude of the hysteresis increases with the polydispersity and thickness (MW) of the brush layer. With increased cycling, the curves collapse to a master interaction force profile that is similar to that expected for a more monodisperse brush system. In other words, with cycling the force is dominated by the osmotic repulsion rather than the details of the brush structure. These findings suggest that the structure of the diffuse outer layer of the brush is greatly modified by compression and takes a significant time to relax back to a more equilibrium state. Osaki et al.[71] developed an empirical formula to calculate the relaxation time of a polymer in semi-dilute solution by modeling the dynamic modulus using the Rouse model. Using this method, the relaxation time over our polymer MW range is on the order of 10^{-2} seconds - much faster than the experimental time scale of the force profile measurements. Indeed, the experimental time scale is over three orders of magnitude longer, but still not sufficient for the system to equilibrate. The entanglement MW of PS in melt is ~18 Kg/mole,[72] and increases with decreasing polymer volume fraction with a -4/3 power.[46, 73] All the studied ATRP brushes are above the entanglement MW. In contrast, most physisorbed brushes formed by grafting-to method are below the entanglement MW once the polymer volume fraction is accounted for. This is consistent

with the fact that the highly hysteric behavior was only observed with the ATRP brushes, but no any noticeable hysteresis in the force profile measurements was observed between cycles over similar time scales for the 50:50 PS-P2VP diblock brush (PS MW 57k).

3.4.3 *Shear Force Measurements*

Lateral shear force measurements were carried out on the thickest ATRP brush layer, Σ~162. In particular, we were very interested in determining the friction behavior as this brush system had the highest hysteresis in the compression cycles. Figure 5 plots both the normal and shear force as a function of separation between the brush layers. Again, the high hysteresis in the normal force profiles demonstrate that the experimental time scale is shorter than the relaxation process of the brush layer. Surprisingly, lateral shear force was undetectable within the experimental resolution until the opposing layers were highly-compressed. This demonstrates that these polydisperse brushes provide an excellent lubrication layer. Even at a volume fraction of only 34% toluene the effective friction coefficient of the layers was less than 0.02. It is commonly suggested that the friction force between polymer brush layers originates from viscous dissipation within the mutual interpenetration region of the opposing polymer brushes.[29, 30] Based on MD simulations, Spirin et al.[74] have suggested that two types of entanglements need to be taken into consideration in polymer brush systems during sliding; intra-brush entanglements inside an individual brush layer and inter-brush entanglements that occur between the opposing brush layers. As no adhesion was observed between the brush layers during force compression measurements, the findings suggest that intra-brush entanglements within each brush layer increase during compression. These intra-brush

entanglements are more dominate than inter-brush entanglements between the two brushes which reduces opposing brush interpenetration and enables low friction sliding between the brushes even under high compression. This important intra-brush entanglement behavior is consistent with the observation of Ruths et al.[37]

The low friction sliding of these ultra-high density brushes is even more remarkable given the low solvation of the brushes. The friction force between the brushes only becomes measurable when the volume fraction of toluene drops below 34%. After this point, the friction rapidly increases as the brushes are further compressed. Kobayashi et al.[42] also

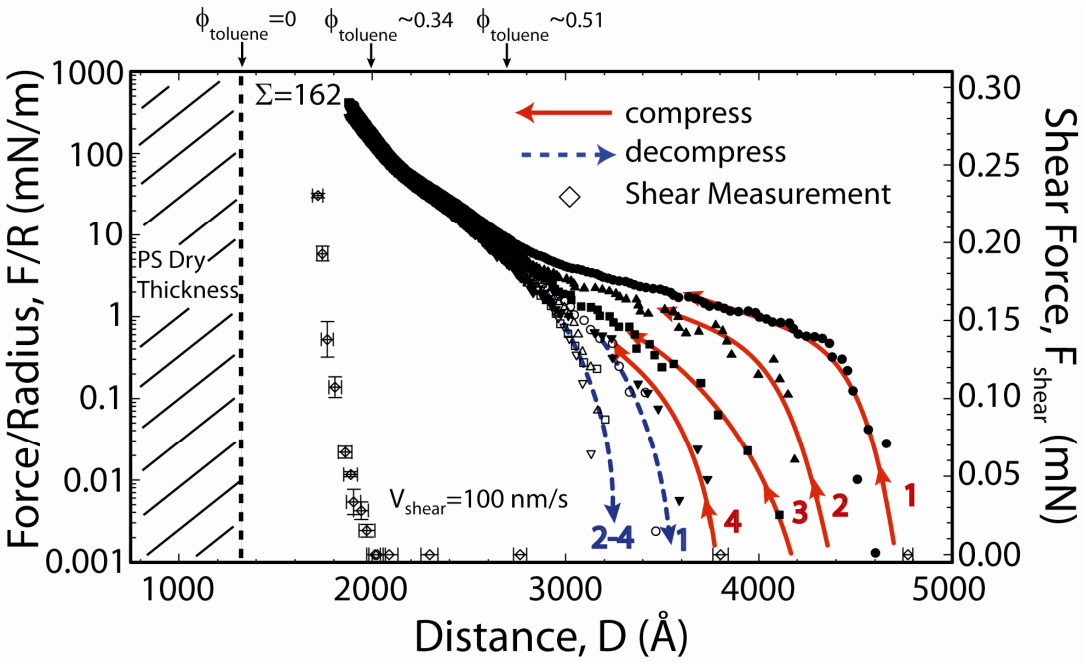

Figure 5. Normal and shear forces as a function of separation between two opposing ATRP grown PS brushes with Σ=162 in toluene. Four compression (closed symbols) / decompression (open symbols) cycles are shown. The solid and dashed lines are the guides to the eye for the different compression/decompression cycles. Shear force measurements (2nd Y axis) were carried out with a velocity of 0.1 μm/s and sliding distance of1.25μm.

observed better lubricant performance for high density P(MPC) brushes in reduced solvent conditions. In this case, the friction was significantly lower in a high-humidity environment compared to that when fully hydrated in water. Similar to the argument presented here, Kobayashi et al. suggested that inter-brush contacts and greater interpenetration occurred in bulk water compared to high humidity conditions.

An important consideration for understanding the properties of high density brushes is possible changes in solvent quality with compression. All the brush systems reported here greatly exceed the semi-dilute regime. Thus, as the brushes are compressed and the polymer concentration in the gap between the surfaces increases, the solvent quality can be significantly reduced resulting in more favorable polymer contacts.[75] This is consistent with more intra- and inter-brush contacts. In addition, the reduction in the solvent quality will substantially decrease the extension of the polymer brushes, which may also reduce the interpenetration region.[31, 32] For higher grafting densities (Σ=111 and 162), the observed force profiles can be reasonably divided into two distinct concentration ranges: a highly hysteretic region and a reversible region after multiple compressions. These regions correspond to less dense outer brush layer and more dense or collapsed inner brush layer, respectively. The denser region could be possibly attributed to the entanglement network formed during the process of chain-transfer termination when the polymerization was conducted at higher temperature[69] while other “escaped” chains continue growing linearly and created a less dense outer region. Without sufficient relaxation time, the extension of the brush from the dense region is greatly diminished presumably due to formation of favorable intra-brush contacts under solvent starved conditions. Likewise, inter-brush contacts become more favorable and

with high compression ($\Phi<35\%$) and the friction increases rapidly. For lower compressions the outer region of the brush layers remain well solvated and provide frictional properties similar to semi-dilute brushes that have been commonly studied in the past.

3.5 Conclusion

Both normal and shear interactions between ultra-high grafted polymer brushes have been examined in the present work. Very long relaxation times are evident from the observed hysteresis with compression separation cycles. The hysteresis increases with increasing brush polydispersity. Remarkably, the friction behavior is found to be very similar to low density brushes in the semi-dilute regime and does not increase appreciably until the solvent volume fraction is less than 35%. The importance of the high density brushes yielding favorable lubrication properties is that a highly durable lubricating layer can be formed. These findings demonstrate that high grafting density brushes with high polydispersity – a real system rather than ideal monodisperse system – have potential as lubricants in more practical applications.

3.6 References

1. Klein, J., et al., *Lubrication forces between surfaces bearing polymer brushes.* Macromolecules, 1993. **26**(21): p. 5552-5560.
2. Brochard-Wyart, F., et al., *Adhesion promoters.* J. Phys. Chem., 1994. **98**(38): p. 9405-9410.
3. Devaux, C., et al., *Controlled structure and density of "living" polystyrene brushes on flat silica surfaces.* The European Physical Journal E - Soft Matter, 2002. **7**(4): p. 345-352.
4. Milner, S.T., *Polymer Brushes.* Science, 1991. **251**(4996): p. 905-914.
5. de Gennes, P.G., *Conformations of Polymers Attached to an Interface.* Macromolecules, 1980. **13**(5): p. 1069-1075.
6. Zhao, B. and W.J. Brittain, *Polymer brushes: surface-immobilized macromolecules.* Progress in Polymer Science, 2000. **25**(5): p. 677-710.
7. Kent, M.S., et al., *Tethered chains in good solvent conditions: An experimental study involving Langmuir diblock copolymer monolayers.* The Journal of Chemical Physics, 1995. **103**(6): p. 2320-2342.
8. Goujon, F., P. Malfreyt *, and D.J. Tildesley, *The compression of polymer brushes under shear: the friction coefficient as a function of compression, shear rate and the properties of the solvent.* Molecular Physics, 2005. **103**(19): p. 2675-2285.
9. Devaux, C., et al., *Low Swelling Capacity of Highly Stretched Polystyrene Brushes.* Macromolecules, 2005. **38**(10): p. 4296-4300.

10. Alexander, S., *Adsorption of Chain Molecules with a Polar Head a-Scaling Description.* Journal De Physique, 1977. **38**(8): p. 983-987.

11. Alexander, S., *Polymer adsorption on small spheres: A scaling approach.* Journal de physique., 1977. **38**(8): p. 977-982.

12. De Gennes, P.G., *Polymer solutions near an interface. Adsorption and depletion layers.* Macromolecules, 1981. **14**(6): p. 1637-1644.

13. Milner, S.T., T.A. Witten, and M.E. Cates, *A Parabolic Density Profile for Grafted Polymers.* EPL (Europhysics Letters), 1988. **5**(5): p. 413-418.

14. Milner, S.T., T.A. Witten, and M.E. Cates, *Theory of the grafted polymer brush.* Macromolecules, 1988. **21**(8): p. 2610-2619.

15. Taunton, H.J., et al., *Interactions between surfaces bearing end-adsorbed chains in a good solvent.* Macromolecules, 1990. **23**(2): p. 571-580.

16. Kilbey, S.M., et al., *Direct Force and Friction Measurements Reflecting Structural Changes in Confined Diblock Copolymer Liquids.* Macromolecules, 1995. **28**(16): p. 5626-5631.

17. Kilbey, S.M., H. Watanabe, and M. Tirrell, *Structure and Scaling of Polymer Brushes near the theta Condition.* Macromolecules, 2001. **34**(15): p. 5249-5259.

18. Alonzo, J., J.W. Mays, and S.M. Kilbey Ii, *Forces of interaction between surfaces bearing looped polymer brushes in good solvent.* Soft Matter, 2009. **5**(9): p. 1897-1904.

19. Kent, M.S., et al., *Characterization of diblock copolymer monolayers at the liquid-air interface by neutron reflectivity and surface tension measurements.* Macromolecules, 1992. **25**(23): p. 6240-6247.

20. Baranowski, R. and M.D. Whitmore, *Numerical self-consistent field study of tethered chains in Theta solvent.* The Journal of Chemical Physics, 1998. **108**(23): p. 9885-9892.

21. Baranowski, R. and M.D. Whitmore, *Theory of the structure of adsorbed block copolymers: Detailed comparison with experiment.* The Journal of Chemical Physics, 1995. **103**(6): p. 2343-2353.

22. Grest, G.S., *Grafted polymer brushes in polymeric matrices.* The Journal of Chemical Physics, 1996. **105**(13): p. 5532-5541.

23. Grest, G.S., *Grafted polymer brushes: a constant surface pressure molecular dynamics simulation.* Macromolecules, 1994. **27**(2): p. 418-426.

24. Pastorino, C., et al., *Static and dynamic properties of the interface between a polymer brush and a melt of identical chains.* J. Chem. Phys., 2006. **124**(6): p. 064902.

25. Elliott, I.G., T.L. Kuhl, and R. Faller, *Molecular Simulation Study of the Structure of High Density Polymer Brushes in Good Solvent.* Macromolecules, 2010. **43**(21): p. 9131-9138.

26. Klein, J., et al., *Reduction of frictional forces between solid surfaces bearing polymer brushes.* Nature, 1994. **370**(6491): p. 634-636.

27. Klein, J., D. Perahia, and S. Warburg, *Forces between polymer-bearing surfaces undergoing shear.* Nature, 1991. **352**(6331): p. 143-145.

28. Raviv, U., R. Tadmor, and J. Klein, *Shear and Frictional Interactions between Adsorbed Polymer Layers in a Good Solvent.* The Journal of Physical Chemistry B, 2001. **105**(34): p. 8125-8134.

29. Klein, J., et al., *Shear forces between sliding surfaces coated with polymer brushes: The high friction regime.* Acta Polymerica, 1998. **49**(10-11): p. 617-625.

30. Tadmor, R., et al., *Sliding Friction with Polymer Brushes.* Physical Review Letters, 2003. **91**(11): p. 115503.

31. Schorr, P.A., et al., *Shear Forces between Tethered Polymer Chains as a Function of Compression, Sliding Velocity, and Solvent Quality.* Macromolecules, 2003. **36**(2): p. 389-398.

32. Forster, A.M., J.W. Mays, and S.M. Kilbey, *Effect of temperature on the frictional forces between polystyrene brushes.* Journal of Polymer Science Part B: Polymer Physics, 2006. **44**(4): p. 649-655.

33. Grest, G.S., *Interfacial Sliding of Polymer Brushes: A Molecular Dynamics Simulation.* Physical Review Letters, 1996. **76**(26): p. 4979-4982.

34. Witten, T.A., L. Leibler, and P.A. Pincus, *Stress relaxation in the lamellar copolymer mesophase.* Macromolecules, 1990. **23**(3): p. 824-829.

35. Kreer, T., et al., *Frictional Drag Mechanisms between Polymer-Bearing Surfaces.* Langmuir, 2001. **17**(25): p. 7804-7813.

36. Ejaz, M., et al., *Controlled Graft Polymerization of Methyl Methacrylate on Silicon Substrate by the Combined Use of the Langmuir−Blodgett and Atom Transfer Radical Polymerization Techniques.* Macromolecules, 1998. **31**(17): p. 5934-5936.

37. Ruths, M., et al., *Repulsive Forces and Relaxation on Compression of Entangled, Polydisperse Polystyrene Brushes.* Macromolecules, 2000. **33**(10): p. 3860-3870.

38. Milner, S.T., T.A. Witten, and M.E. Cates, *Effects of polydispersity in the end-grafted polymer brush.* Macromolecules, 1989. **22**(2): p. 853-861.

39. Yamamoto, S., et al., *Surface Interaction Forces of Well-Defined, High-Density Polymer Brushes Studied by Atomic Force Microscopy. 1. Effect of Chain Length.* Macromolecules, 2000. **33**(15): p. 5602-5607.

40. Yamamoto, S., et al., *Surface Interaction Forces of Well-Defined, High-Density Polymer Brushes Studied by Atomic Force Microscopy. 2. Effect of Graft Density.* Macromolecules, 2000. **33**(15): p. 5608-5612.

41. de Gennes, P.G., *Polymers at an interface; a simplified view.* Advances in Colloid and Interface Science, 1987. **27**(3-4): p. 189-209.

42. Kobayashi, M., et al., *Friction behavior of high-density poly(2-methacryloyloxyethyl phosphorylcholine) brush in aqueous media.* Soft Matter, 2007. **3**(6): p. 740-746.

43. Sakata, Y., et al., *Tribological Properties of Poly(methyl methacrylate) Brushes Prepared by Surface-Initiated Atom Transfer Radical Polymerization* Polym. J., 2005. **37**(10).

44. Kobayashi, M. and A. Takahara, *Synthesis and Frictional Properties of Poly(2,3-dihydroxypropyl methacrylate) Brush Prepared by Surface-initiated Atom Transfer Radical Polymerization.* Chemistry Letters, 2005. **34**(12): p. 1582.

45. Dunlop, I.E., et al., *Direct Measurement of Normal and Shear Forces between Surface-Grown Polyelectrolyte Layers†.* The Journal of Physical Chemistry B, 2009. **113**(12): p. 3947-3956.

46. Colby, R.H., M. Rubinstein, and J.L. Viovy, *Chain entanglement in polymer melts and solutions.* Macromolecules, 1992. **25**(2): p. 996-998.

47. Vigil, G., et al., *Interactions of Silica Surfaces.* Journal of Colloid and Interface Science, 1994. **165**(2): p. 367-385.

48. Matyjaszewski, K., et al., *Polymers at Interfaces: Using Atom Transfer Radical Polymerization in the Controlled Growth of Homopolymers and Block Copolymers from Silicon Surfaces in the Absence of Untethered Sacrificial Initiator.* Macromolecules, 1999. **32**(26): p. 8716-8724.

49. Ell, J.R., et al., *Structural Determination of High Density, ATRP Grown Polystyrene Brushes by Neutron Reflectivity.* Macromolecules, 2009. **42**(24): p. 9523-9527.

50. Xia, J. and K. Matyjaszewski, *Controlled/"Living" Radical Polymerization. Atom Transfer Radical Polymerization Using Multidentate Amine Ligands.* Macromolecules, 1997. **30**(25): p. 7697-7700.

51. Israelachvili, J.N., *Thin film studies using multiple-beam interferometry.* Journal of Colloid and Interface Science, 1973. **44**(2): p. 259-272.

52. Israelachvili, J.N. and G.E. Adams, *Direct measurement of long range forces between two mica surfaces in aqueous KNO3 solutions.* Nature, 1976. **262**(5571): p. 774-776.

53. Israelachvili, J.N. and G.E. Adams, *Measurement of forces between two mica surfaces in aqueous electrolyte solutions in the range 0–100 nm.* J. Chem. Soc., Faraday Trans., 1978. **1**(74): p. 975 - 1001.

54. Israelachvili, J.N. and M. McGuiggan, *Adhesion and short-range forces between surfaces. Part I: New apparatus for surface force measurements.* J. Mater. Res., 1990. **5**.

55. Parker, J.L., H.K. Christenson, and B.W. Ninham, *Device for measuring the force and separation between two surfaces down to molecular separations.* Review of Scientific Instruments, 1989. **60**(10): p. 3135-3138.

56. Derjaguin, B.V., Kolloid Zeits, 1934. **69**: p. 155-164.

57. Israelachvili, J., *direct measurement of forces between surfaces in liquids at the molecular level.* Proc. Natl. Acad. Sci. USA, 1987. **84**: p. 4722-4724.

58. Luengo, G., et al., *Thin Film Rheology and Tribology of Confined Polymer Melts: Contrasts with Bulk Properties.* Macromolecules, 1997. **30**(8): p. 2482-2494.

59. Clarkson, M.T., *Multiple-beam interferometry with thin metal films and unsymmetrical systems.* Journal of Physics D: Applied Physics, 1989. **22**(4): p. 475.

60. Orozco-Alcaraz, R. and T. Kuhl, *Interaction forces between DPPC bilayers on glass.* Manuscript to be submitted for publication.

61. Biesalski, M. and J. Rühe, *Scaling Laws for the Swelling of Neutral and Charged Polymer Brushes in Good Solvents.* Macromolecules, 2001. **35**(2): p. 499-507.

62. Biesalski, M. and J. Rühe, *Preparation and Characterization of a Polyelectrolyte Monolayer Covalently Attached to a Planar Solid Surface.* Macromolecules, 1999. **32**(7): p. 2309-2316.

63. Wu, T., et al., *Behavior of Surface-Anchored Poly(acrylic acid) Brushes with Grafting Density Gradients on Solid Substrates: 1. Experiment.* Macromolecules, 2007. **40**(24): p. 8756-8764.

64. Higo, Y., N. Ueno, and I. Noda, *osmotic pressure of semidilute solutions of branched polymers.* polymer journal, 1983. **15**(5): p. 367-375.

65. Milner, S.T., *Compressing polymer brushes—a quantitative comparison of theory and experiment.* Europhysics Letters, 1988. **7**: p. 695-699.

66. Kim, J.U. and M.W. Matsen, *Compression of Polymer Brushes: Quantitative Comparison of Self-Consistent Field Theory with Experiment.* Macromolecules, 2009. **42**(9): p. 3430-3432.

67. Liao, W.-P. and T.L. Kuhl, *Steric Forces of Tethered Polymer Chains as a Function of Grafting Density: Studies with a Single Diblock Molecular Weight.* Macromolecules, 2012.

68. Noda, I., et al., *Semidilute region for linear polymers in good solvents.* Macromolecules, 1984. **17**(5): p. 1055-1059.

69. Samadi, A., et al., *Low-Temperature Growth of Thick Polystyrene Brushes via ATRP.* Macromolecular Rapid Communications, 2005. **26**(23): p. 1829-1834.

70. Israelachvili, J.N., R.K. Tandon, and L.R. White, *Measurement of forces between two mica surfaces in aqueous polyethylene oxide solution.* Journal of Colloid and Interface Science, 1980. **78**(2): p. 430-443.

71. Osaki, K., et al., *Evaluation methods of the longest Rouse relaxation time of an entangled polymer in a semidilute solution.* Journal of Polymer Science Part B: Polymer Physics, 2001. **39**(14): p. 1704-1712.

72. Onogi, S., T. Masuda, and K. Kitagawa, *Rheological Properties of Anionic Polystyrenes. I. Dynamic Viscoelasticity of Narrow-Distribution Polystyrenes.* Macromolecules, 1970. **3**(2): p. 109-116.

73. Tao, H., C.-i. Huang, and T.P. Lodge, *Correlation Length and Entanglement Spacing in Concentrated Hydrogenated Polybutadiene Solutions.* Macromolecules, 1999. **32**(4): p. 1212-1217.

74. Spirin, L., et al., *Polymer-brush lubrication in the limit of strong compression.* The European Physical Journal E: Soft Matter and Biological Physics, 2010. **33**(4): p. 307-311.

75. Zhou, Z.W. and P.J. Daivis, *Molecular dynamics study of polymer conformation as a function of concentration and solvent quality.* Journal of Chemical Physics, 2009. **130**(22): p. 224904-1~224904-10.

Chapter 4: Other Techniques and Analysis

4.1 Structure characterization of polymer brushes in confinement cell

When two surfaces bearing polymer brushes are brought together, two behaviors may happen at the same time: interpenetration and compression. Although direct measurement of the interaction forces between two opposing brush layers can be provided by SFA, the internal structure of the tethered chains or the molecular mechanisms involved in the transition of the forces is not attainable. The single-surface structure of polymer brushes in different solvent conditions as a function of grafting density has been extensively investigated by neutron reflectivity [1-8]. For opposing layers in confined geometries, the difficulty lies in the need of adequately large, ultra-flat surfaces for neutron experiments as well as parallel and aligned interspacing between the surfaces during the measurements [4]. Different confinement cell devices which can fulfill this demand have been proposed for specific measurements [9-11]. In addition, better modeling capabilities are required to deal with the incoherent scattering which must be taken into consideration as there are always variations in the level of confinement between the two opposing surfaces.

Figure 1 shows the Neutron Confinement Cell (NCC) utilized for structure examination of opposing brushes and more details have been previously described elsewhere.[10] Briefly, the two chosen substrates coated with desired polymer brush layers are placed in a polymer-to-polymer geometry in a reservoir which can be filled with solvent. The two

opposing surfaces are then brought together by applying hydraulic pressure. Using this approach, a separation between the substrates on the order of 1000 angstroms could be achieved. The same environment as that in the SFA experiments described in chapter 2 was reproduced and the SFA measured force profiles were compared to the structure of the confined polymer brushes under similar conditions as measured by neutron reflectivity. The method of preparing the samples was the same for the two measurement techniques, but the substrates are quartz, Silicon wafer or sapphire for neutron reflectivity measurements instead of mica as used in SFA measurements. The structure information was extracted by fitting the measured reflectivity profile using the MIRROR program. The details of the analysis procedures can be found in chapter 2.

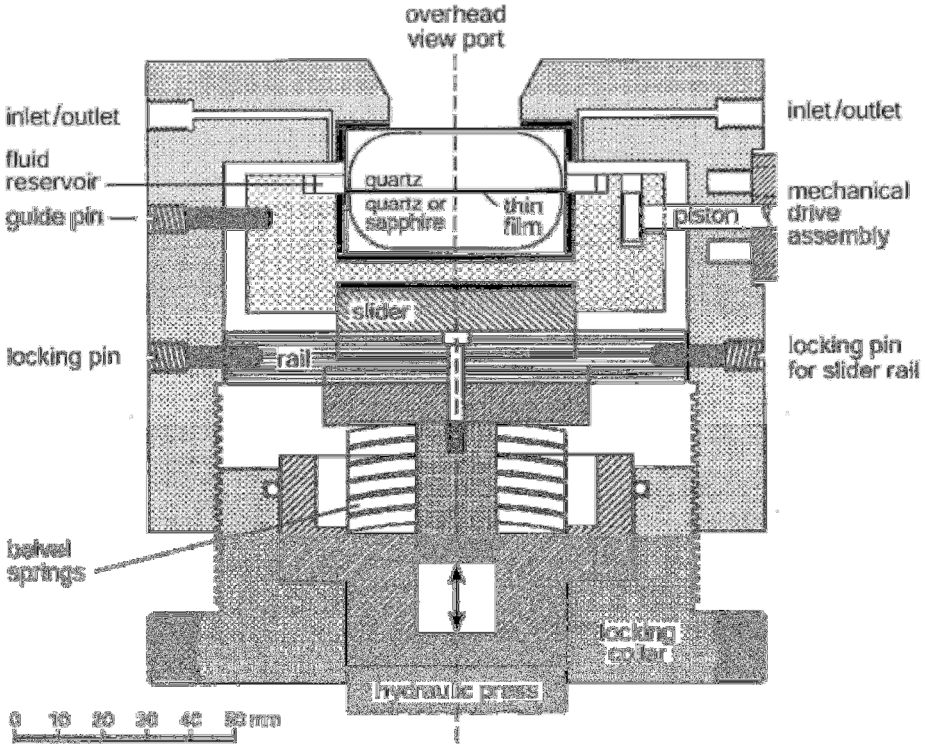

Figure 1. Cross sectional view of the Neutron Confinement Cell (NCC).[10]

I. Deuterated Polystyrene (dPS) – Deuterated Polystyrene (dPS)

The following analysis demonstrates the structure of opposing polymer brushes studied by neutron reflectivity with NCC. The 1 wt% deuterated polystyrene solution was spin-coated on different substrates (quartz and sapphire) for better contrast in the fitting process.

The air measurement was done first to confirm the amount of polymer and also how well the Polystyrene (PS) and Polyvinylpyridine (P2VP) were segregated after the annealing process. After determining the distance of the air gap, the opposing films were fully

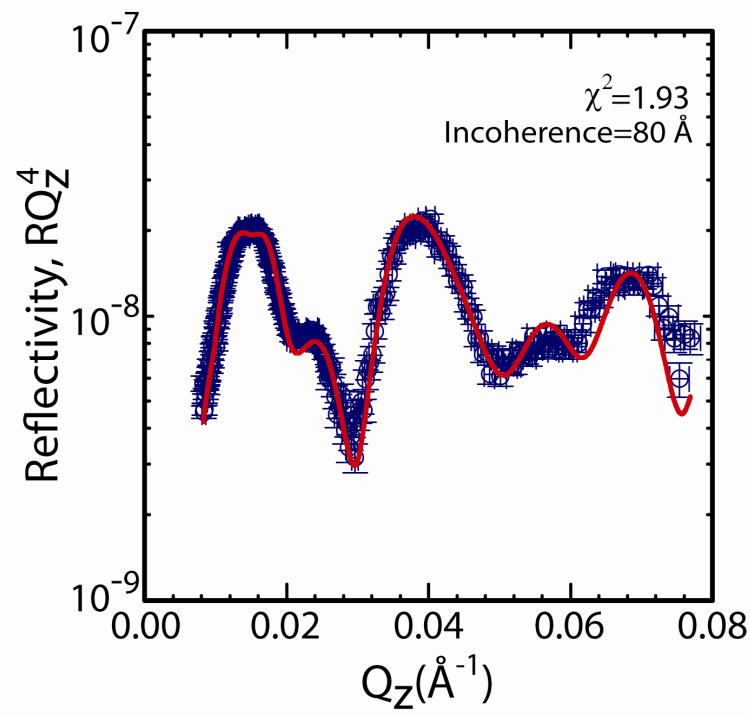

Figure 2. The raw reflectivity data of dPS-dPS system and the quality of the fit was demonstrated by chi square.

solvated with toluene. Figure 2 shows the best fit in air and the corresponding structure is plotted in figure 3. To obtain the best quality of the fit which was determined by the smallest chi squared value between the reflectivity data and the model profile, an incoherence length of 80Å was incorporated in the model setting. In figure 3, PS and P2VP was shown fully separated and the air gap was 586Å.

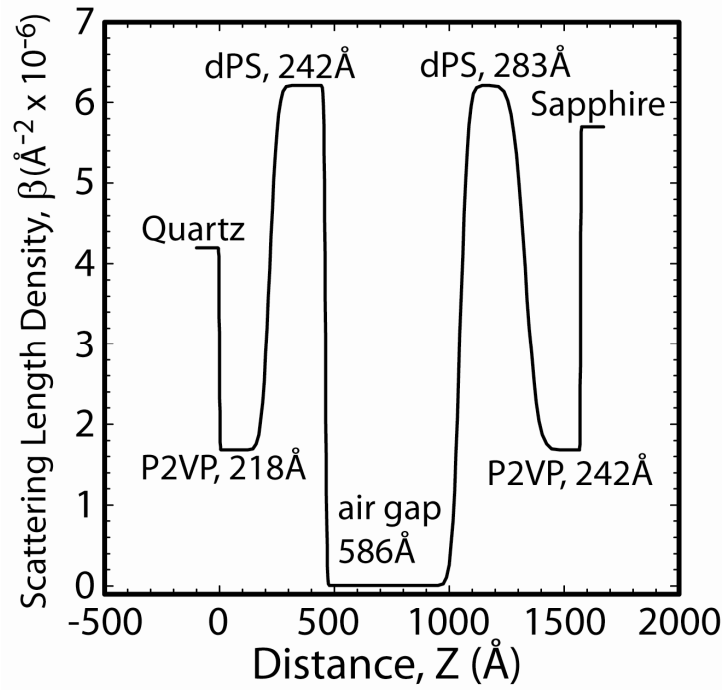

Figure 3. The corresponding scattering length density profile of the best fit in air.

However, during the fitting process, distinguishing the contribution between the incoherence and air gap on the reflectivity was not an easy task. In figure 4, the incoherence was fixed at 30Å while it was 60 Å for figure 5. Different air gap spacing was altered to show how it will change the fit. Unfortunately, both of the effects will smooth out the curve and also comprise the fit.

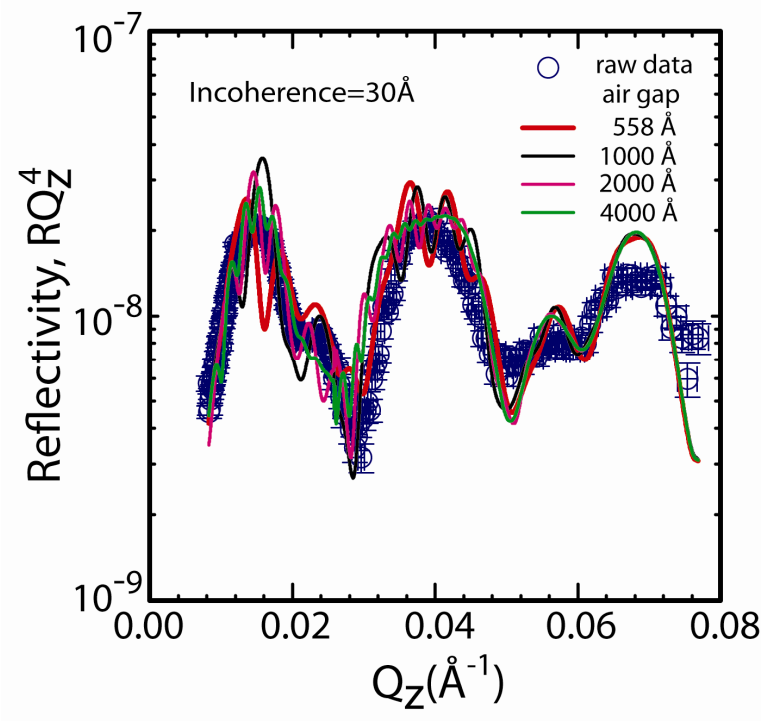

Figure 4. Fits of different air gaps for incoherence=30Å.

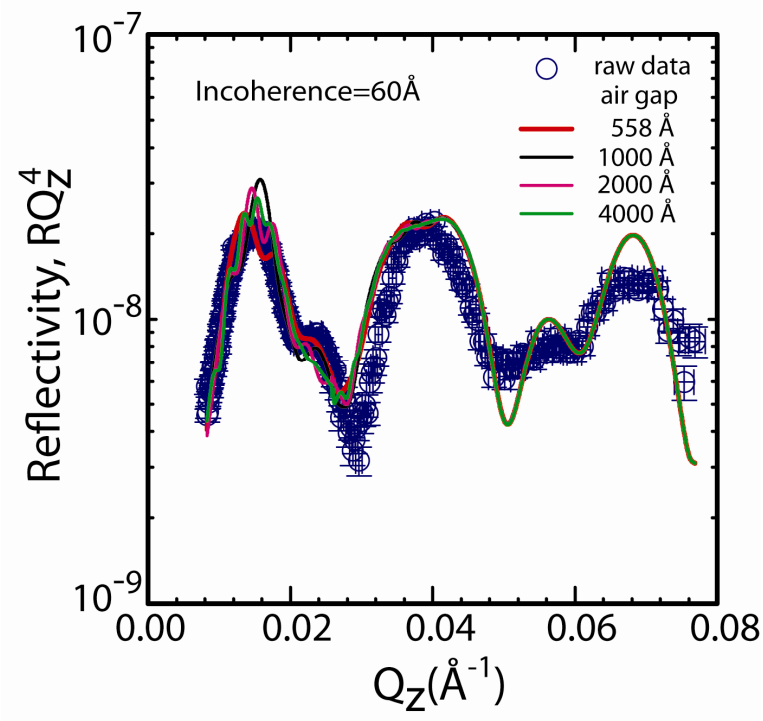

Figure 5. Fits of different air gaps for incoherence=60Å.

To further compare the measured reflectivity both in air and in solvent in figure 6, the rough length scale in the system can be estimated by the scattering vector difference between neighboring peaks or valleys using $d=2\pi/\Delta Q$. The spacing between the layers was confirmed to be around 1750 Å and this is beyond what was expected. The difficulties in determining the gap and incoherence length have stopped further analysis.

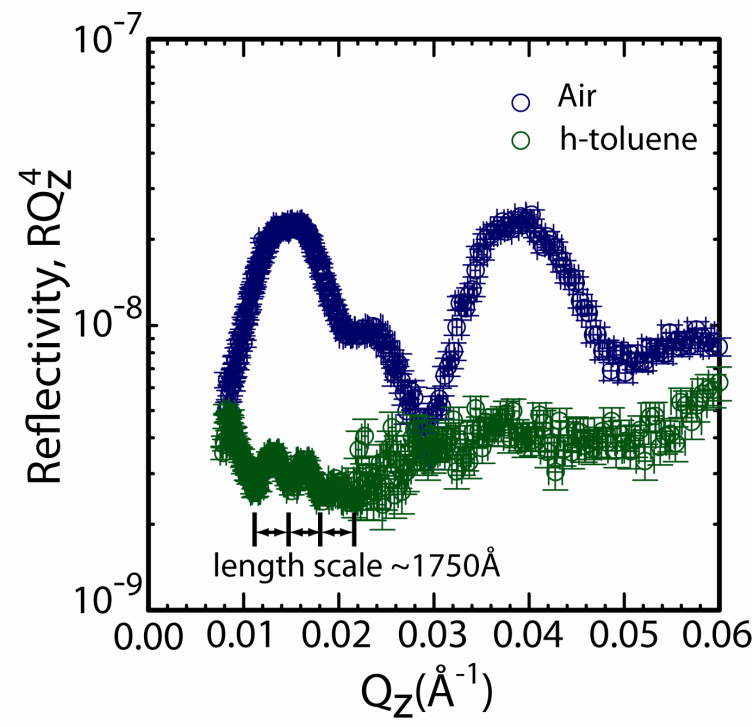

Figure 6. Comparison between reflectivity data in air and solvent conditions.

II. Deuterated Polystyrene (dPS) – hydrogenated Polystyrene (hPS)

The structure of opposing brushes with one side of hPS and the other side of dPS was also measured. After the air experiment, the whole setting was solvated in the contrast-match-hPS toluene (10 wt% d-toluene + 90 wt% h-toluene) to more easily examine where the tails of the dPS brushes extended. In figure 7, different incoherence lengths were considered to achieve the best fit quality and the scattering length density (SLD) profile of the best fit in air is shown in Figure 8. With increasing coherence length, lower chi square value could be obtained. Figure 9 demonstrates the raw reflectivity data when in a solvated environment and the best fit was found with an incoherence length=60Å and the corresponding SLD model is plotted in Figure 10. However, the same problem described previously for the dPS-dPS system was also observed when distinguishing between the contribution of the spacing and the incoherence length. This complication makes analyzing the data extremely difficult. In addition, the stability of the film was another concern when determining the right fitting model due to the observation of some polymer film desorption when similar films were solvated in SFA experiments. Although the amount of the solvent used was different in SFA (340mL) and the NCC (10mL), the binding force between the substrate and the polymer plays a very important role in dictating the level of desorption. As a result, further modification of the polymer or the tethering mechanism (changing system) are necessary before the structure of the confined polymer brush system can be more accurately and confidently determined.

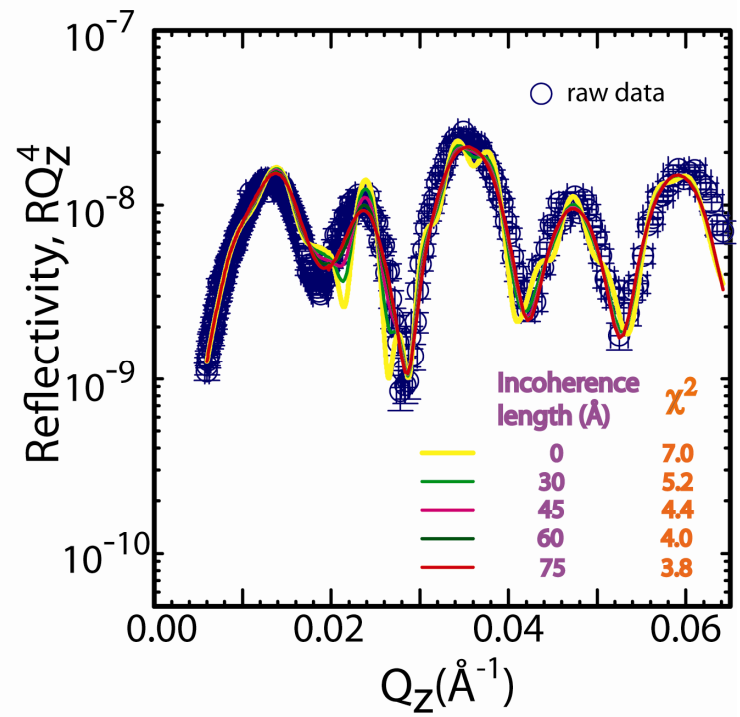

Figure 7. The raw reflectivity data of dPS-hPS system was demonstrated and how the quality of the fits altered with incoherence length.

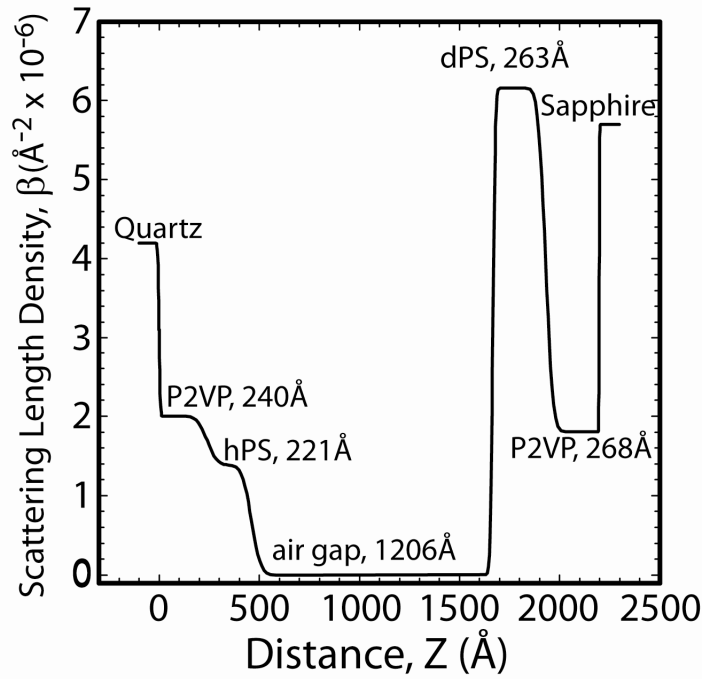

Figure 8. The corresponding scattering length density profile of the best fit in air.

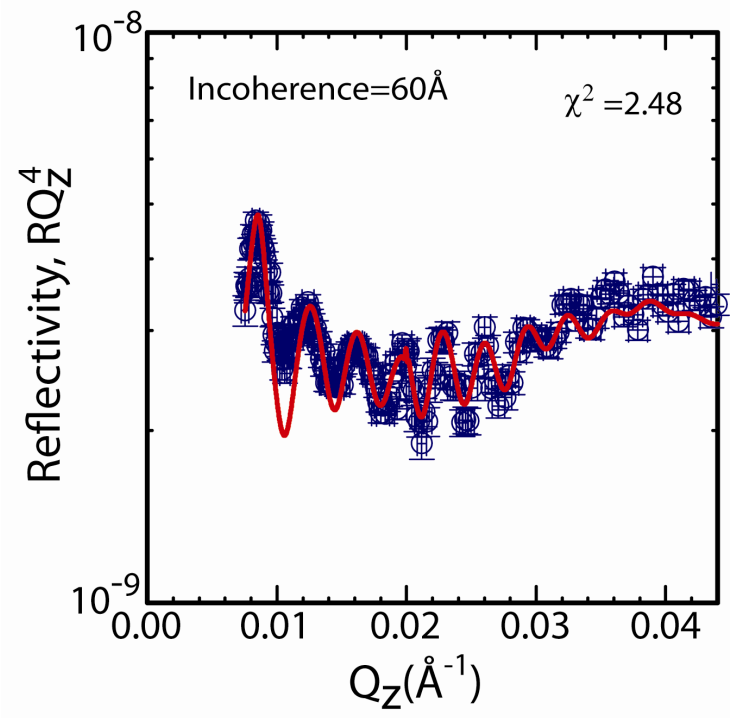

Figure 9. The raw data of the solvated dPS-hPS system and the best fit.

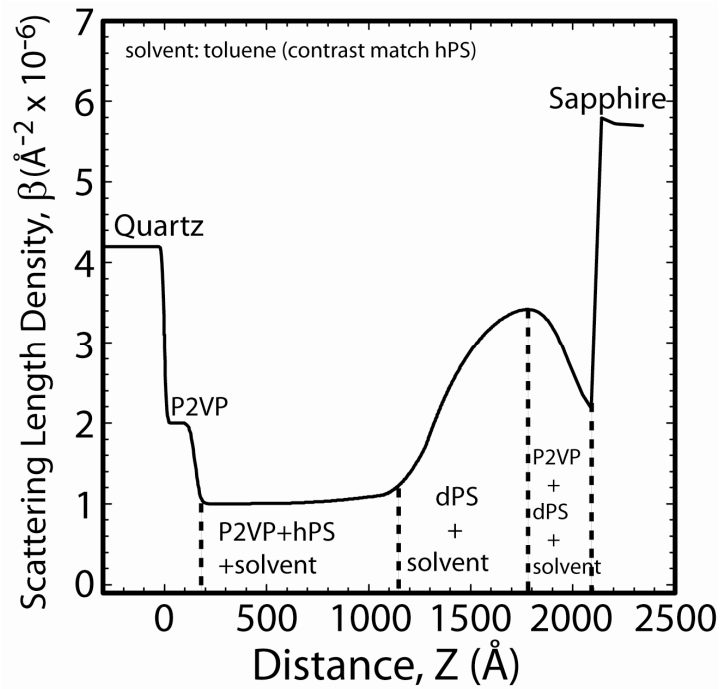

Figure 10. The corresponding scattering length density profile of the best fit in solvent.

4.2 Shear and Normal forces between physisorbed polymer brushes.

In addition to the normal interactions in chapter 2, the shear force between two opposing polymer brushes formed by physical adsorption methods was also measured. The same block copolymer PS-P2VP (57K-57K) was used and the sample preparation was the same as has been described in chapter 2. The shear measurements were accomplished following the setting mentioned in chapter 3 with all other parameters remaining the same. The sliding velocity was 100nm/s through the duration of the measurements and the sliding distance was 1.25 μm. The calculated grafting density was 0.0013 chains/$Å^2$. Figure 11 shows both the normal force and the shear force as a function of distance and the inset shows a schematic of the experimental brush system. The shear force was first detectable with our instrument resolution when the volume fraction of solvent is around 0.72. This is a lot different from what was observed for higher grafting density brushes formed by ATRP methods in chapter 3. One thing that should be noticed is the effective friction coefficient in this set of experiments was also larger than that measured for the ATRP brushes. Unfortunately, there is a possibility that some loss of polymer occurs during the shear measurements. Due to film stability issues no further conclusion can be reached and more durable polymer brush films with different types of binding energies would be highly recommended for studying the shear response for brush systems to avoid this potential complication.

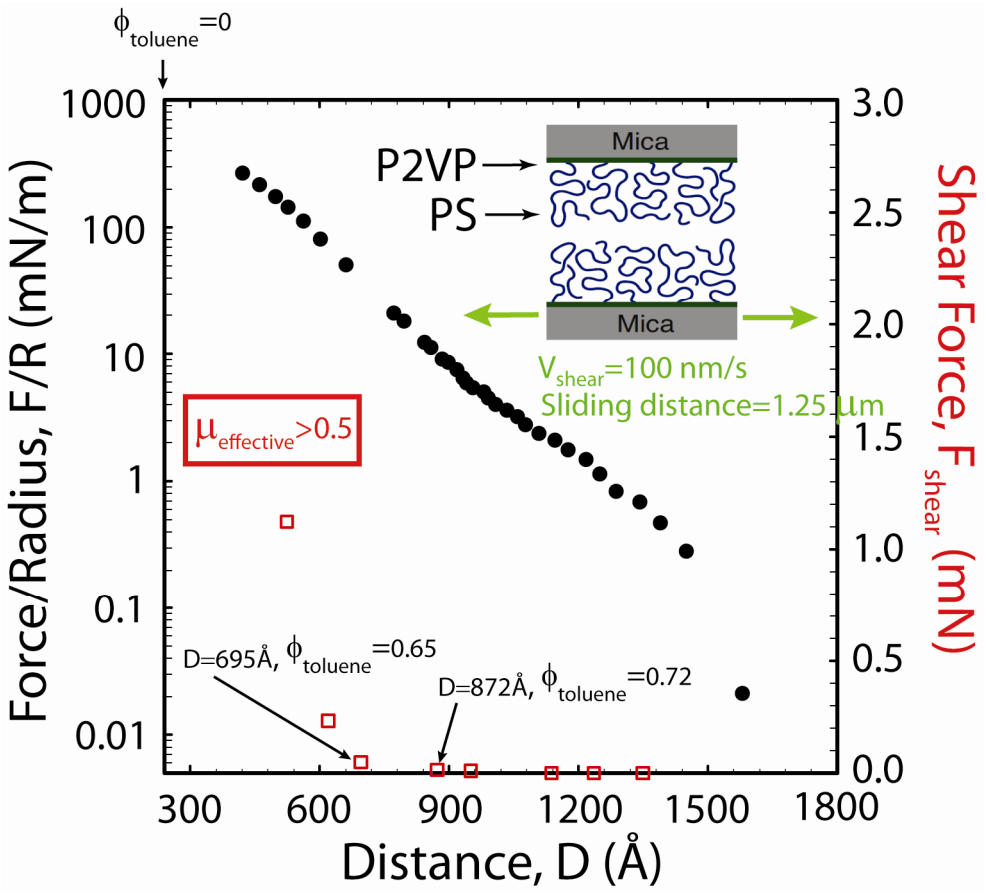

Figure 11. Normal and shear forces as a function of separation between two opposing physisorbed brushes in toluene. The inset shows a schematic of the experimental brush system.

4.3 A shear device for neutron reflectometry to measure the structure and shear behavior simultaneously

The experimental structure determination using the reflectivity technique under shear that has been reported previously was either for unconfined polymer brushes at a single interface [12-14] or just compression with normal load.[15] Load-plus-shear treatment to polymer at the same time in the confinement cell has not been done. The idea here is to have the ability to probe the structure of the polymer brush layer under shear and compare to the SFA friction force under shear. Different theoretical predictions about the equilibrium thickness of polymer brushes under shear are very diverse. It ranges from no changes in the brush extension [16, 17] to obvious increase[18-20], while some even predict a decrease in extension of layer thickness[21, 22]. As a result, experimental data is needed to test the accuracy of the theoretical models. In previous experiments [12-14], the shear was accomplished by solvent flow past the polymer brush layer. In order to verify the theoretical calculation, higher shear rates are desirable. However, even though shear rates of 10 kHz can be reached, the systems studied so far remained in the laminar flow regime. In addition, the measurements were accomplished for only one brush layer against bulk solvent Data measured under both normal load and shear movement for opposing polymer brushes is required to compare with theoretical predictions and SFA measurements. Moreover, this geometry of opposing surfaces reflects actual applications where polymer films are used to provide a lubricating layer between two sliding surfaces (e.g. human joints). The confinement cell previously described works well for probing the structure of opposing brushes under compression but the shear option does not. So far, no experimental work has successfully measured the structure of opposing polymer

brushes with both normal and shear loading simultaneously. Consequently, to design a device which can fulfill this demand would be very useful and certainly very challenging.

The initial approach of the design is to build up a motor-rotated disk which can withstand high load similar to a tribometer. Using this method, a large substrate will be rotated relative to a small surface the size of the neutron beam foot print. Both the rotary disk and the other surface can be spin coated with polymer. The smaller bottom surface will be located on the outer edge of the large, rotating disk. The controlled rpm of the disk can be converted to an approximately linear shear as the angular range of this orientation is relatively small. In other words, if the upper rotating disk is sufficiently large relative to the bottom surface, one can assume that the whole bottom surface is subjected to the same shear rate. Although the velocity will vary depending on the radius, the error can be less than 10% according to calculations. The major difficulty lies in the ability to keep the interspacing stable during the high shear rate rotation, this issue may be solved by using an air bearing device. The stability can be determined by an empty experiment just like the test method in confinement cell design.[10] In this design, the fact that substrates “slide” laterally past one another is different from the shear motion caused by the solvent flow passing the brush surface. As a result, comparing the results between two shear mechanisms will be very informative.

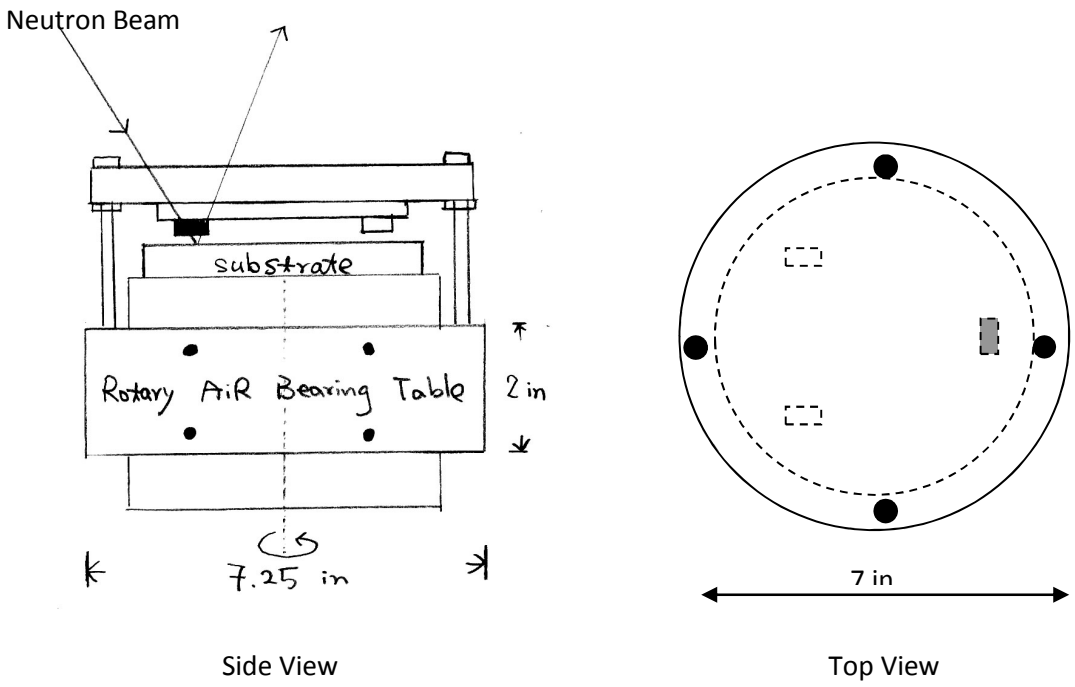

Figure 12. A rough sketch of proposed Load-plus-shear neutron reflectivity device.

Reference

1. Kent, M.S., et al., *Tethered chains in good solvent conditions: An experimental study involving Langmuir diblock copolymer monolayers.* The Journal of Chemical Physics, 1995. **103**(6): p. 2320-2342.
2. Russell, T.P., *X-ray and neutron reflectivity for the investigation of polymers.* Materials Science Reports, 1990. **5**(4): p. 171-271.
3. Devaux, C., et al., *Controlled structure and density of "living" polystyrene brushes on flat silica surfaces.* The European Physical Journal E - Soft Matter, 2002. **7**(4): p. 345-352.
4. Hamilton, W.A., et al., *Determining the density profile of confined polymer brushes with neutron reflectivity.* Journal of Polymer Science Part B: Polymer Physics, 2004. **42**(17): p. 3290-3301.
5. Devaux, C., et al., *Low Swelling Capacity of Highly Stretched Polystyrene Brushes.* Macromolecules, 2005. **38**(10): p. 4296-4300.
6. Levicky, R., PhD Thesis, University of Minnesota, Minneapolis, Minnesota, 1996.
7. Levicky, R., et al., *Concentration Profiles in Densely Tethered Polymer Brushes.* Macromolecules, 1998. **31**(11): p. 3731-3734.
8. Perahia, D., et al., *Neutron reflectivity of end-grafted polymers: Concentration and solvent quality dependence in equilibrium conditions.* Physical Review Letters, 1994. **72**(1): p. 100.

9. Cosgrove, T., et al., *Adsorption of polystyrene–poly (ethylene oxide) block copolymers on quartz using a parallel-plate surface-force apparatus and simultaneous neutron reflection.* Farady Discuss, 1994. **98**: p. 189-201.

10. Kuhl, T.L., et al., *Neutron confinement cell for investigating complex fluids.* Review of Scientific Instruments, 2001. **72**(3): p. 1715-1720.

11. Cosgrove, T., et al., *The measurement of volume fraction profiles for adsorbed polymers under compression using neutron reflectometry.* Colloids and Surfaces A: Physicochemical and Engineering Aspects, 1994. **86**: p. 103-110.

12. Nguyen, D., et al., *Investigation of Polymer Brushes and Adsorbed Layers under Shear.* Journal of Applied Crystallography, 1997. **30**(5 Part 2): p. 680-683.

13. Baker, S.M., et al., *Shear cell for the study of liquid-solid interfaces by neutron scattering.* Review of Scientific Instruments, 1994. **65**(2): p. 412-416.

14. Baker, S.M., et al., *Structure of Polymer Brushes under Shear Flow in a Good Solvent.* Macromolecules, 2000. **33**(4): p. 1120-1122.

15. Mulder, D.J. and T.L. Kuhl, *Polymer brushes in restricted geometries.* Soft Matter, 2010. **6**(21): p. 5401-5407.

16. Rabin, Y. and S. Alexander, *Stretching of Grafted Polymer Layers.* EPL (Europhysics Letters), 1990. **13**(1): p. 49-54.

17. Miao, L., H. Guo, and M.J. Zuckermann, *Conformation of Polymer Brushes under Shear: Chain Tilting and Stretching.* Macromolecules, 1996. **29**(6): p. 2289-2297.

18. Barrat, J.L., *A possible mechanism for swelling of polymer brushes under shear.* Macromolecules, 1992. **25**(2): p. 832-834.

19. Aubouy, M., J.L. Harden, and M.E. Cates, *Shear-Induced Deformation and Desorption of Grafted Polymer.* J. Phys. II, 1996. **6**: p. 969-.

20. Harden, J.L. and M.E. Cates, *Deformation of grafted polymer layers in strong shear flows.* Physical Review E, 1996. **53**(4): p. 3782.

21. Doyle, P.S., E.S.G. Shaqfeh, and A.P. Gast, *Rheology of "Wet" Polymer Brushes via Brownian Dynamics Simulation: Steady vs Oscillatory Shear.* Physical Review Letters, 1997. **78**(6): p. 1182.

22. Saphiannikova, M.G., V.A. Pryamitsyn, and T. Cosgrove, *Self-Consistent Brownian Dynamics Simulation of Polymer Brushes under Shear.* Macromolecules, 1998. **31**(19): p. 6662-6668.